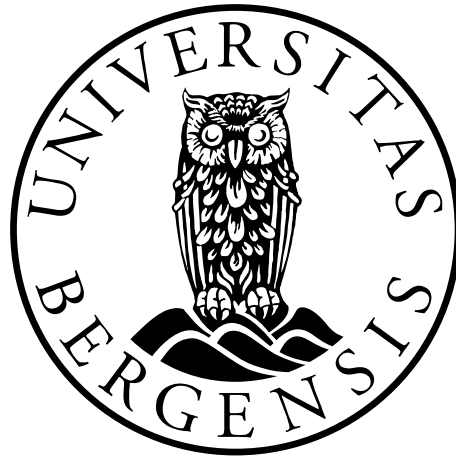# Correlations between the effective permeability and seismic anisotropy of fractured reservoirs

Aamir Ali

Dissertation for the degree philosophiae doctor (PhD)

Department of Earth Science

University of Bergen

Norway

June, 2011

Abstract

The successful exploitation of many hydrocarbon reservoirs may depend on proper characterization of fractured or composite porous media. However, due to anisotropy and heterogeneity, the characterization of such kind of reservoirs is a complicated task which needs proper attention and care. There are often strong correlations between the effective permeability and seismic anisotropy of fractured reservoirs. The exploitation of such correlations is extremely important in understanding of the spatial variation of anisotropic permeability. The purpose of this thesis work was to develop novel workflows and methodologies in order to exploit the correlations between effective permeability and seismic anisotropy of fractured reservoirs.

The correlations between the effective mechanical and transport properties of fractured reservoirs within the context of a joint inversion of seismic and production data have been exploited to obtain improved hydrocarbon reservoir characterization. In this work, the effective mechanical and transport properties of fractured reservoirs and related systems are estimated using an efficient and consistent permeability-stiffness model from the same parameters of microstructure. The estimated effective mechanical properties in combination with anisotropic Gassmann relations have been used to calculate the seismic amplitude versus angle and azimuth AVAZ) data i.e. reflection coefficients as a function of incidence angle and azimuth from the top of the reservoir. Similarly from the estimated effective hydraulic properties, the reservoir simulator can calculate the production data such as well bottom hole pressure, well oil production, well water cut, saturation and pressure for all grid blocks at specific time steps.

The seismic AVAZ and/or production data is used in the Bayesian inversion scheme to estimate the parameters of factures (e.g. fracture density, fracture aperture and fracture orientation) required to predict permeability. This work shows that joint inversion of seismic and production data give the best results due to the less sensitivity of seismic AVAZ data to fracture aperture which is one of the most

important parameter of the microstructure predicting the permeability. This workflow of joint inversion of seismic and production data has also been applied for the characterization of faulted reservoirs (e.g., fault damage zone with deformation bands oriented parallel to the fault core). The transmissibility multiplier is used to model the effect of the fault core and the consistent rock physics model has been used to model fractures and deformation bands in the damaged zone.

Analogies between different physical phenomena and coupled processes such as wave-induced fluid flow have been given a special attention to infer more useful information about fractured reservoirs containing single or multiple sets of fractures. In this context, implications of the unified theory for the relative importance of global and squirt flow characterized by different microstructures and fluid mobilities are invesigated. This work shows that global flow effects are not so important at seismic frequencies for more realistic models of microstructure and needs very high permeability and low viscosity to have an effect.

For the case of a fractured reservoir containing a single set of fractures, it is demonstrated in this work that an improved characterization can indeed be obtained from frequency-dependent seismic AVAZ data, provided that the anisotropic Gassmann relations are replaced by a theory for seismic attenuation and dispersion due to wave-induced fluid flow. The reflection coefficients are no longer assumed to be real-valued and frequency-independent. The information about all the three fracture parameters can be obtained that determine the effective permeability tensor.

For the case of complex fractured reservoirs (with multiple fracture sets), it is demonstrated in this work that measurements of velocity anisotropy data corresponding to different seismic frequencies and azimuths alone cannot recover the parameters related with multiple sets of fractures i.e. the fracture densities and the azimuthal fracture orientations. Joint inversion of measurements of seismic velocity and attenuation anisotropy data corresponding to different seismic frequencies and azimuths leads to improved estimates of fracture parameters and better management

of fractured reservoirs containing multiple sets of fractures. A satisfactory characterization of complex fractured reservoirs requires a model accounting for frequency-dependent anisotropy.

The results obtained form these workflows and methods can help in better management of fractured reservoirs and optimum field development.

Preface

The thesis is submitted in partial fulfillment of the degree philosophiae doctor in Petroleum Geosciences at the Department of Earth Sciences at the University of Bergen. The research was mainly funded by the Higher Education Commission (HEC) Pakistan and partially by the Department of Earth Sciences University of Bergen. This project is linked to a larger Center of Integrated Petroleum Research (CIPR) project (task 3a) dealing with reservoir monitoring and characterization with production, seismic and electromagnetic data. I have focused more on seismic and production part of the project.

The thesis work was mostly conducted at the University of Bergen. The principle supervisor for this project was Associate Professor Morten Jakobsen at the University of Bergen, and the co-supervisor was Senior Engineer Bent Ole Ruud at the University of Bergen.

This dissertation is divided into two parts along with their appendices:

Part I (Introduction): This part focuses on the general theoretical background and methodology used in this study and describes the main scientific contributions that make up the main body of the thesis.

Part II (Papers): The second part presents a collection of six research papers, which is the main outcome of my study. Out of these six papers, first three papers are published online and the rest has been submitted and are in review in international peer-review journals.

Papers

Paper 1: Ali, A., and Jakobsen, M. (2011): 'On the accuracy of Rüger's approximations for reflection coefficients in HTI media: Implications for the determination of fracture density and orientation from seismic AVAZ data', Journal of Geophysics and Engineering, Published online.

Paper 2: Ali, A., Shahraini, A., and Jakobsen, M. (2011): 'Improved characterization of fault zones by quantitative integration of seismic and production data', Journal of Geophysics and Engineering, Published online.

Paper 3: Shahraini, A., Ali, A., Jakobsen, M., (2010): 'Characterization of fractured reservoirs using a consistent stiffness-permeability model: focus on the effects of fracture aperture, Geophysical Prospecting, Published online (also printed in hard copy).

Paper 4: Ali, A., and Jakobsen, M. (2011): 'On the relative importance of global and squirt flow in cracked porous media', Geophysical Journal International, Submitted.

Paper 5: Ali, A., and Jakobsen, M. (2011): 'Anisotropic permeability in fractured reservoirs from frequency-dependent seismic AVAZ data', Geophysical Prospecting, Submitted.

Paper 6: Ali, A., and Jakobsen, M. (2011): 'Seismic characterization of reservoirs with multiple fracture sets using velocity and attenuation anisotropy data', Journal of Applied Geophysics, Submitted.

Appendices (Part II)

Extended Abstract 1: Ali, A., Shahraini, A., and Jakobsen, M. (2009): 'Improved characterization of fault zones by quantitative integration of seismic and production data', 6129, EAGE Annual Meeting Amsterdam.

Extended Abstract 2: Ali, A., and Jakobsen, M. (2010): 'On the accuracy of Rüger's Approximations for PP Reflection Coefficients in HTI Media', 8334, EAGE Annual Meeting Barcelona.

Extended Abstract 3: Shahraini, A., and Jakobsen, M., and Ali. A. (2010): 'Seismic History Matching in Fractured Reservoirs Using a Consistent Stiffness-permeability Model - Focus on the Aperture', K035, EAGE Annual Meeting Barcelona.

Extended Abstract 4: Ali, A., and Jakobsen, M. (2011): 'On the Relative Importance of Global and Squirt Flow in Cracked Porous Media', 10981, EAGE Annual Meeting Vienna.

Extended Abstract 5: Ali, A., and Jakobsen, M. (2011): 'Seismic characterization of reservoirs with multiple fracture sets using velocity and attenuation anisotropy data', 10650, EAGE Annual Meeting Vienna.

Acknowledgements

I express my deep gratitude to my principal advisor 'Morten Jakobsen' for making this PhD thesis possible. I am thankful for his inspiration, continuous support, encouragement and excellent guidance during my PhD studies. I am always thankful to him for accepting me as his PhD student. I am thankful for the support during the difficult times of this PhD work.

I am also grateful to my co-supervisor 'Bent Ole Ruud' for his help during my PhD studies.

I would also like to thank my PhD colleague Ali Shahraini for all the constructive discussion on the topics related to my PhD study. Special thanks go to him for co-operation on our joint papers.

My deepest thanks go to Higher Education Commission (HEC) of Pakistan and Department of Earth Sciences, University of Bergen for creating the opportunity to study abroad and providing the necessary funding to complete the work. I also acknowledge my employer Quaid-I-Azam University (QAU), Islamabad, Pakistan and Department of Earth Sciences, QAU, Islamabad, Pakistan to approve my study leave to complete this PhD study. I would also like to thank my friends at Bergen. We had many unforgettable happy moments during this stay.

Finally, special thanks go to my family (brothers/brothers in law and sisters/sisters in law), nieces (Madikh, Maryam, Hajra, Zayan, Taish and Uzair) and my parents along with my elder brother (Dr. Nasir Ali) who built me so high with their wounded hands. Thanks for always been there.

Aamir Ali

June 2011

Contents

PART II. PAPERS

PAPER 1. ON THE ACCURACY OF RÜGER'S APPROXIMATION FOR REFLECTION COEFFICIENTS IN HTI MEDIA: IMPLICATIONS FOR THE DETERMINATION OF FRACTURE DENSITY AND ORIENTATION FROM SEISMIC AVAZ DATA.

PAPER 2. IMPROVED CHARACTERIZATION OF FAULT ZONES BY QUANTITATIVE INTEGRATION OF SEISMIC AND PRODUCTION DATA.

PAPER 3. CHARACTERIZATION OF FRACTURED RESERVOIRS USING A CONSISTENT STIFFNESS-PERMEABILITY MODEL: FOCUS ON THE EFFECTS OF FRACTURE APERTURE.

PAPER 4. ON THE RELATIVE IMPORTANCE OF GLOBAL AND SQUIRT FLOW IN CRACKED POROUS MEDIA.

PAPER 5. ANISOTROPIC PERMEABILITY IN FRACTURED RESERVOIRS FROM FREQUENCY-DEPENDENT SEISMIC AVAZ DATA.

PAPER 6. SEISMIC CHARACTERIZATION OF RESERVOIRS WITH MULTIPLE FRACTURE SETS USING VELOCITY AND ATTENUATION ANISOTROPY DATA.

APPENDICES (PART II) – PEER-REVIEWED EXTENDED ABSTRACTS

APPENDIX-1. IMPROVED CHARACTERIZATION OF FAULT ZONES BY QUANTITATIVE INTEGRATION OF SEISMIC AND PRODUCTION DATA

APPENDIX-2. ON THE ACCURACY OF RÜGER'S APPROXIMATION FOR PP REFLECTION COEFFICIENTS IN HTI MEDIA.

APPENDIX-3. SEISMIC HISTORY MATCHING IN FRACTURED RESERVOIRS USING A CONSISTENT STIFFNESS-PERMEABILITY MODEL - FOCUS ON THE APERTURE.

APPENDIX-4. ON THE RELATIVE IMPORTANCE OF GLOBAL AND SQUIRT FLOW IN CRACKED POROUS MEDIA.

APPENDIX-5. SEISMIC CHARACTERIZATION OF RESERVOIRS WITH MULTIPLE FRACTURE SETS USING VELOCITY AND ATTENUATION ANISOTROPY DATA.

Part I. INTRODUCTION

1. Overview

A large and increasing percentage of world's hydrocarbon reserves need the evaluation of fractured (carbonate) reservoirs (Nelson, 2001). Carbonate reservoirs hold approximately 60% of the world's petroleum reserves, accounting for 40% of the total hydrocarbon production (Chopra et al., 2005). The extraction of hydrocarbons present in fractured rocks is a growing target of exploration and development and the proper characterization of fractures is of increasing concern for the petroleum industry due to its complex and unconventional reservoir architecture (Steve et al., 2000). This suggests the need of finding new methods to successfully identify and characterize fracture networks that often provide pathways for hydrocarbon flow and also play a significant role in the successful secondary recovery of the resources (Steve et al., 2000). Fracture networks have a significant effect on reservoir fluid flow either in terms of increased reservoir permeability or increased reservoir permeability anisotropy. The understanding of the spatial variations of anisotropic permeability becomes a crucial issue for the management of fractured reservoirs.

There are often strong correlations between the effective permeability and seismic anisotropy of fractured reservoirs. Historically, there have been relatively few attempts to make use of such correlations in the context of fractured reservoir characterization (but see King, 2002; MacBeth and Pickup, 2002; Rogers et al., 2003; Will et al., 2005; Rasolofosaon and Zinszner, 2002; Pyrak-Nolte and Morris, 2000; Jakobsen et al., 2007a, b; Shahraini et al., 2010). More specifically, seismic anisotropy can be used to determine the orientation of fractures (Sayers 2009). The exploitation of such correlations is extremely important in understanding of the spatial variation of anisotropic permeability in fractured reservoirs.

The uncertainty in parameters related to fractures increases with increasing distance from the borehole. Three-dimensional seismic data provide uncalibrated information throughout the inter-well space that needs to be properly calibrated and up-scaled (Will et al., 2005). A seismic wave propagating or a fluid flowing through a fractured

reservoir can only see a homogenized structure and not the individual fractures, because the wavelength of the seismic wave or the scale-size of the pressure variations is often much larger than the scale-size of the fractures. The calibration and up-scaling of information from seismic measurements can be obtained through a good understanding of relevant rock physics modelling associated with fractures and composite porous media (Jakobsen et al., 2003a, b; Jakobsen, 2007a, b and c). The fractured reservoir may therefore in many cases be replaced with an effective homogenous medium for the purpose of seismic or fluid-flow modelling. The effective homogenous medium will be anisotropic if the fractures are oriented in a preferred direction. Rock physics models may also represent a kind of regularization within the context of seismic inversion or history matching. History matching is a process of updating a reservoir model to behave as closely as possible to the conditions of a real reservoir.

Figure 1 represents a schematic workflow diagram for estimation of fracture parameters from seismic amplitude versus angle and azimuth (AVAZ) data. The parameters of fractures (e.g., fracture density and azimuthal fracture orientation) for each grid block are updated until the objective function is minimized. The inversion has been done in a Bayesian setting, which provides information about the uncertainties and as well as single estimates or most likely values of the fracture parameters. When the parameters of the fractures are known, one could obtain the estimates of the effective permeability tensors using a consistent rock physics model for effective hydraulic properties. This workflow is followed in paper 1 of this PhD thesis within the context of seismic fracture characterization.

Seismic AVAZ inversion in the context of fractured reservoir characterization using the workflow presented in figure 1 may provide improved permeability estimates from seismic anisotropy, if one makes simple assumptions about the fracture geometry. For example fracture aperture, which is an important parameter controlling the fluid flow during production (Liu et al., 2005), having a little effect on the seismic

response in the absence of squirt flow (local pressure gradients). This suggests two approaches to obtain more improved characterization of fractured reservoirs.
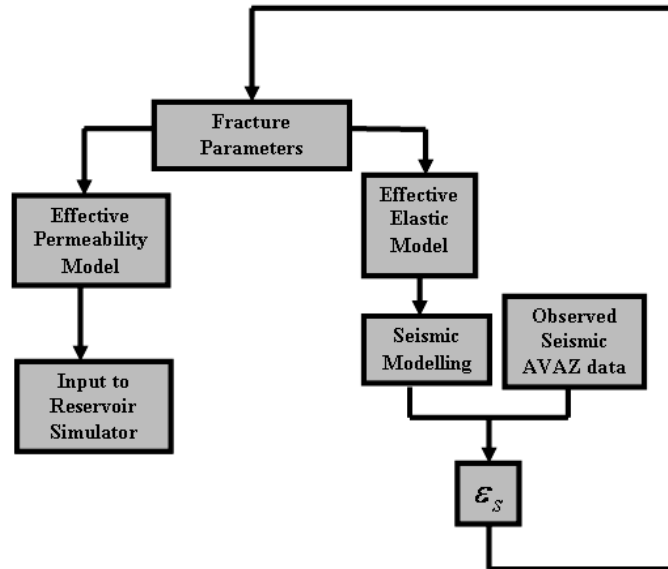

Figure 1 Schematic workflow diagram for the estimation of fracture parameters from seismic AVAZ inversion.

The first approach deals with an integration of data type sensitive to fracture geometry in the workflow such as production data and a joint inversion of seismic and production data should be performed. Figure 2 represents a schematic workflow diagram for estimation of the fracture parameters by the quantitative integration of seismic and production data. The static (e.g., fracture density, the fracture orientation and the fracture aperture) and dynamic parameters of fractures (e.g., saturation) for each grid block are updated until the joint (related with integration of seismic and production data) objective function is minimized.

The workflow described in figure 2 is applied in paper 2 and 3 of this PhD thesis. In paper 2 we focus on the characterization of faulted reservoirs. The transmissibility multiplier is used to model the effect of the fault core and a consistent rock physics model has been used to model fractures and/or deformation bands in the damaged zone. The parameters related to fault core and/or deformation bands are estimated by the joint inversion of seismic and/or production data. In paper 3, the workflow is

followed within the context of fractured reservoir characterization and seismic history matching.
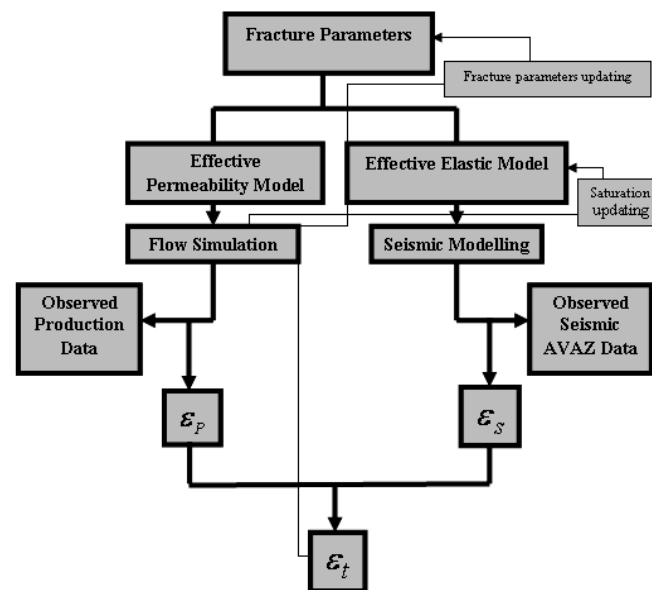

Figure 2 Schematic workflow diagram for the estimation of fracture parameters by quantitative integration of seismic AVAZ and production data.

The second approach deals with the analysis of seismic anisotropy data using a model which can incorporate seismic attenuation and dispersion due to wave induced fluid flow. Wave induced fluid flow can occur in the form of global and/or squirt flow. Global flow, also known as Darcy flow, is caused by pressure gradients at the scale of the seismic wavelength and in the direction of wave propagation, whereas squirt flow is caused by the pressure gradients at the microscopic or mesoscopic scale and in the direction potentially different from that of the wave propagation. The presence of mesoscopic fractures in a reservoir can produce significant dispersion and attenuation at seismic frequencies, suggesting that it is generally not safe to treat seismic frequencies as the low frequency limit (Maultzsch et al., 2003; Gurevich et al., 2009). Measurements related to frequency dependence of seismic anisotropy or seismic velocity and attenuation anisotropy data can potentially give important information about the fracture systems and fluid saturation (Chapman, 2003; Liu et al., 2007a, b; Maultzsch et al., 2007; Chapman, 2009; Clark et al., 2009).

Figure 3 represents a schematic workflow diagram for estimation of fracture parameters by incorporating the seismic attenuation and dispersion due to wave induced fluid flow. The relative importance of global and squirt flow in cracked/fractured porous media characterized by different microstructures and fluid mobilities has also been given attention. A change in viscosity may lead to a shift of the attenuation peak towards lower or higher frequencies, depending on the mechanism of wave induced fluid flow. These issues are addressed in paper 4 of this PhD thesis by investigating the relative importance of global and squirt flow in cracked/fractured porous media.

The workflow presented in figure 3 is followed in paper 5 of this PhD thesis within the context of seismic fracture characterization (reservoir containing single set of fractures) using frequency-dependent seismic AVAZ data. The workflow is also extended to more complex fracture modelling (multiple sets of fractures) within the context of seismic fracture characterization using the measurements of seismic velocity and attenuation anisotropy data corresponding to different seismic frequencies and azimuths (paper 6).
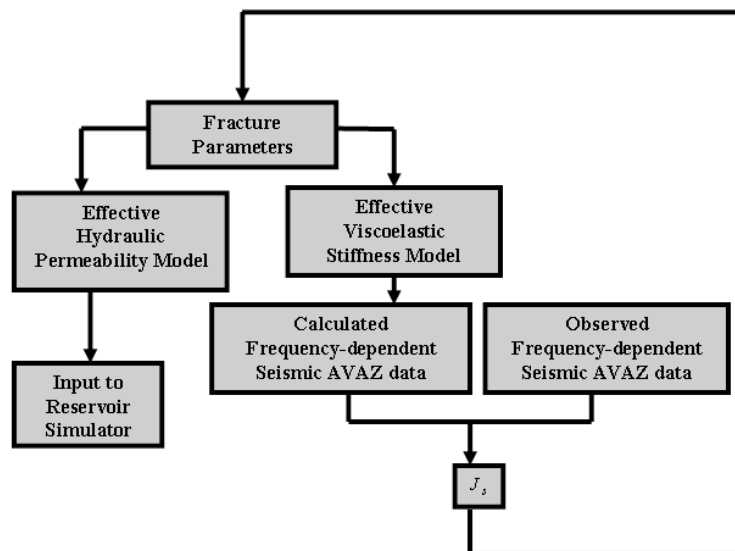
Figure 3 Schematic work flow diagram for estimation of fracture parameters by incorporating the seismic attenuation and dispersion due to wave induced fluid flow.

2. Objectives

The principal aim of this PhD thesis was to obtain a better understanding of the correlations between the effective permeability and stiffness tensors (seismic anisotropy) of fractured reservoirs, so that one can perform improved reservoir simulations with seismically derived fracture models. Special attention was given to exploit the analogies between different physical phenomena and coupled processes such as wave-induced fluid flow to obtain important information about fractured reservoirs containing single or multiple sets of fractures.

A further aim was to investigate various ways of exploiting correlations between the effective mechanical and transport properties of fractured reservoirs within the context of a joint inversion of seismic and production data.

3. Geologic concepts

According to Nelson (2001) the word 'fracture' in a reservoir context can be defined as a naturally occurring macroscopic planar discontinuity in a rock due to deformation and physical digenesis. Based on their deformation properties, the fractures can have a positive, neutral or negative effect on fluid flow in a reservoir (Aguilera, 1995; Nelson, 2001). The above definition of Nelson (2001) also allows addressing the fluid flow anisotropy in fractured reservoirs. A 'fractured' reservoir is defined as a reservoir in which naturally occurring fractures either have, or predicted to have, a significant effect on reservoir fluid either in form of increased reservoir permeability or increased permeability anisotropy (Nelson, 2001).

3.1 Classification of fractures

Fractures can be classified on the basis of their mechanics, genesis and morphology. Based on the mechanics of formation, there are two main types of fractures: extension fractures and shear fractures (Nelson, 2001). Figure 4 show an example of fractures classified on the basis of mechanics of formation. Fractures classified on the basis of genesis are tectonic, regional and contractional or surface related (Nelson, 2001). Figure 5 show an example for the fractures classified on the basis of genesis. Fractures classified according to their morphology are open, mineral filled and vuggy or deformed (Aguilera, 1995; Nelson, 2001). Figure 6 show an example for the fractures classified on the basis morphology.

3.2 Fractures and permeability

The contribution of fractures to permeability largely depends upon their connectivity and also to what degree they link up to make continuous networks (see Van Golf-Racht, 1982; Nelson, 2001; Aguilera, 1995). Fracture connectivity depends upon the

fracture attributes like fracture spacing (also known as fracture density or intensity), aperture (width between walls of the fractures) and length. The effect on fluid flow only becomes important when fractures occur in sufficient spacing or length. Fracture orientation is also another important factor along with these properties to accurately assess the positive or negative effect of fractures on fluid flow.

3.3 Classification of fractured reservoirs

The reservoir must be classified on the basis of what positive effects the fracture system provides to overall reservoir quality (Nelson, 2001). In this regard, the following classification is commonly used:

Type 1: Fractures provide the essential reservoir porosity and permeability.

Type 2: Fractures provide the essential reservoir permeability.

Type 3: Fractures assist permeability in an already producible reservoir.

Type 4: Fractures provides no additional porosity and permeability but create significant reservoir anisotropy.

3.4 Deformation bands

Deformation bands are localized deformation structures that form in highly porous rocks and sediments and commonly found in faulted sand and reservoir-quality sandstone (Torabi and Fossen, 2009). There are different deformation mechanisms responsible for the formation of deformation bands (Fossen et al., 2007). (1) Granular flow involving rolling, sliding and rotation of sand grains result in the formation of disaggregation bands. (2) Grain fracturing, crushing and abrasion result in formation of cataclastic bands. (3) Dissolution and cementation result in the formation of dissolution and cementation bands. Deformation bands are commonly from millimeters to centimeters thick and sometimes up to 100 m long (Sternholf et al.,

2004). They can be observed as a single deformation bands but can also form clusters of deformation bands. As a response to the complicated geometric fault slippages, they can also form and grow in the damage zone of an existing fault (Torabi and Fossen, 2009; Rykkelid and Fossen, 2002). Figure 7 shows an example of the deformation bands in sandstone.
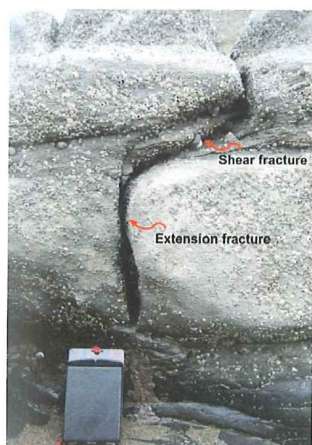
Figure 4 Fracture classified on the basis of mechanics of formation: extension fracture and shear fracture. This figure is taken from the PhD thesis of Larsen (2009).
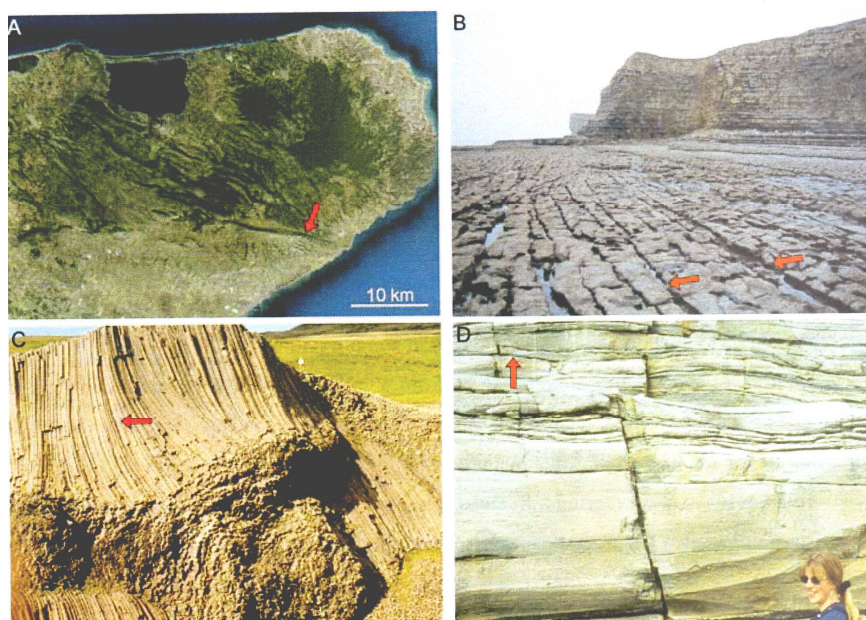
Figure 5 Fractures classified according to their genesis. (A) Tectonic fracture. (B) Regional fractures or joints. (C) Contractional fractures. (D) Surface related fractures. This figure is taken from the PhD thesis of Larsen (2009).
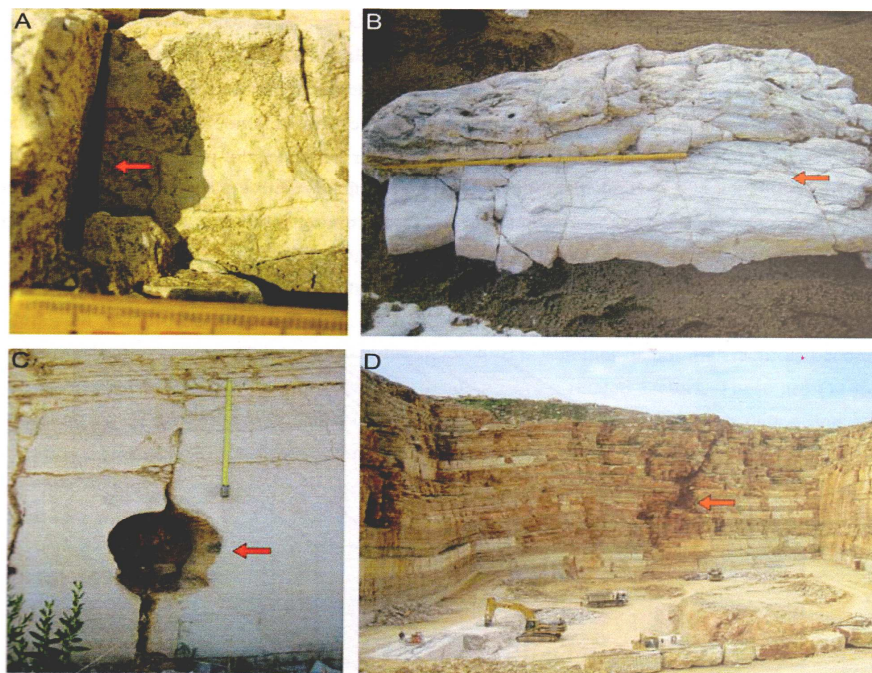
Figure 6 Fractures classified according to their morphology. (A) Open fractures. (B) Mineral filled fractures. (C) Vuggy fractures. (D) Deformed fractures. This figure is taken from the PhD thesis of Larsen (2009).

Figure 7 Deformation bands in Arches National Park Utah. This figure is taken from the master thesis of Kseniya, (2010).

4. Seismic fracture characterization

For carbonate reservoirs, characterizing fractures is an important part of the reservoir development. The goal of the fractured reservoir characterization is to estimate the parameters related with fractures controlling the fluid flow during production. The important parameters of fractures controlling the fluid flow d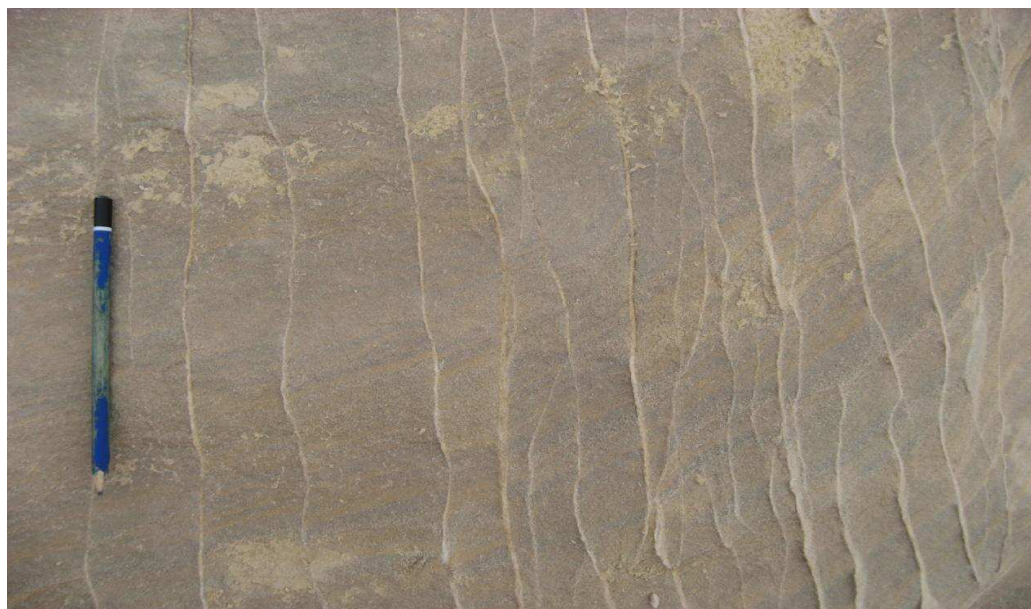uring production are the fracture density, the fracture orientation and the fracture aperture. Once the parameters of the fractures are known, the estimates of the effective permeability can be obtained. Seismic methods are becoming tool of choice from one of the few effective ways of characterizing fractured reservoirs (Steve et al., 2000). The most important seismic attribute is the seismic Amplitude-Versus-Angle and Azimuth (AVAZ) analysis, which captures the information about fractures in a reservoir by detecting the seismic anisotropy caused by fractures (Gray et al., 2002; Downton et al., 2007). Seismic anisotropy is observable in the standard P-wave data recorded over the fractured reservoirs provided that it has sufficient azimuthal and offset coverage (Gray et al., 2002).

For a suitable characterization of fractured reservoirs, all the important fracture parameters controlling the fluid flow should be estimated from seismic AVAZ data. Seismic measurements provide good coverage at depth, but their resolution is lower than the scale of fractures and we cannot directly image the fractures. A similar case occurs in the case of a flowing fluid in a fractured reservoir, the scale-length of pressure variations (the size of a typical grid block in a numerical reservoir simulator) is often much larger than the scale-size of the fractures so that the flowing fluid cannot see the individual fractures. So, to exploit the correlations between the effective permeability and seismic anisotropy of fractured reservoirs, a better understanding of the relevant rock physics and scaling issues is very important. Moreover, rock physics basically provides us a link between seismic and reservoir properties.

4.1 Rock physics modelling

The effect of a fractured layer on the seismic response can be described by anisotropic effective stiffness tensor, which is obtained using anisotropic effective medium theory (Zhang et al., 2009). The effective stiffness tensor for a fractured layer or rock can be estimated by two ways, 1) direct, 2) indirect (Hu and McMechan, 2009). Hu and McMechan (2009) classified the direct effective stiffness methods into single effective inclusion methods (Eshelby, 1957), smoothing methods (Hudson 1980, 1981, 1994), self-consistent methods (O'Connell and Budiansky, 1974; Budiansky and O'Connell, 1976; Willis, 1977; Hoenig, 1979), differential effective medium methods (Nishizawa, 1982; Sheng, 1990; Hornby et al., 1994) and T-matrix methods (Jakobsen et al., 2003a). The indirect methods involve estimation of effective compliance tensor first, from which, effective stiffness tensor can be obtained by inverting the effective compliance tensor. Hu and McMechan (2009) classified the indirect methods into non-interaction approximation (NIA) (Kachanov, 1992; Kachanov et al., 2003; Grechka and Kachanov, 2006a, b, c) and the linear slip (LS) methods (Schoenberg, 1980; Schoenberg and Sayers, 1995; Liu et al., 2000).

These all effective medium theories describe the elastic response of a fractured rock in the long wavelength limit and predict frequency-independent behavior. The presence of mesoscopic fractures in the reservoir can produce significant amount of dispersion and attenuation and these effects cannot be explained by static anisotropic effective medium theories predicting the frequency-independent behavior (Maultzsch et al., 2003). The frequency-dependent anisotropic effective medium theories describing the viscoelastic response of a fractured rock in the long wavelength limit are (e.g. Hudson et al., 1996; Tod, 2001; Chapman, 2003; Jakobsen et al., 2003b; Jakobsen and Chapman, 2009; Gurevich et al., 2009; Müller et al., 2010).

Similarly, the effects of fractures on reservoir fluid flow can be described in terms of an effective reservoir permeability tensor, which is obtained using effective medium theory (Zhang et al., 2009). In reservoir simulation the effective flow properties of a

reservoir containing fractures can also be treated using effective medium theory (Kachanov, 1980; Oda, 1985, Jakobsen 2007c).

The theory of Jakobsen (2007c) for effective permeability is based on the same mathematical formalism (and exactly the same geometrical picture of the fractured reservoir) as the theory of Jakobsen et al., (2003a) or Jakobsen et al., (2003b) for the effective seismic properties representing a consistent model for effective permeability and elasticity of fractured media (Zhang et al., 2009). The T-matrix approach of Jakobsen et al., (2003a, b) also represents the more general computational model that can take account of pores and fractures of any size and aspect ratio (Gurevich et al., 2009; Müller et al., 2010). The model of Chapman (2003) for mesoscopic fractures can be obtained as a limit of the more general T-matrix approach of the Jakobsen et al., (2003b) and Jakobsen and Chapman (2009) (Agersborg et al., 2007; Müller et al., 2010).

Hu and McMechan (2009) argued that it is safer to use an interacting fracture (or inclusion) model such as the higher-order T-matrix approach rather than a non-interacting fracture model (NIA). Both approaches may sometimes give the same predictions, but this depends on the spatial distribution of fractures (see also Ponte Castaneda and Willis 1995). In this thesis I have used the T-matrix approach of Jakobsen et al., (2003a), Jakobsen et al., (2003b), Jakobsen (2007c) and Jakobsen and Chapman (2009) for upscaling the mechanical and hydraulic properties of the fractured and composite porous media. The derivation of T-matrix approach of Jakobsen et al., 2003a, Jakobsen et al., 2003b, Jakobsen and Chapman (2009) and Jakobsen (2007c) is presented in appendix-A, B, C and D. In what follows, I present a comparison of dry case predictions of T-matrix approach, NIA approach and Hudson's (1980, 1981) model for cracked media. The properties of isotropic host rock are taken to be same as given by Hu and McMechan (2009). The crack porosity ϕ is related with the crack density ε by $\phi = (4/3)\pi\varepsilon\alpha$, where α is the aspect ratio for cracks.

Figure 8 show the comparison of dry effective stiffness constant c_{33} obtained using T-matrix approach (Jakobsen et al., 2003a), Hudson's (1980, 1981) model for cracked media and NIA approach (Kachanov et al., 2003; Hu and McMechan, 2009) to the first order in cracked density for a crack model having horizontally transversely isotropic (HTI) symmetry. T-matrix approach and Hudson's model give exactly the same, while overlapping between NIA approach and T-matrix approach at very small fracture densities (< 0.01) is observed, respectively. This shows that the two methods are equivalent at very small crack densities. A very nice description of Hudson's model (1980, 1981) is given in Mavko et al., (2009).

 Figure 9 shows the comparison of a special case of higher order T-matrix approach in which aspect ratio of cracks is equal to aspect ratio of the crack distribution with NIA approach for dry effective stiffness constant c_{33} of a fractured model having HTI symmetry. I have not included the second-order correction of Hudson's model, because second order expansion of Hudson's model is not a uniformly converging series and it predicts increasing moduli with higher crack densities (Cheng, 1993, Mavko et al., 2009). The NIA approach gives exactly the same as higher order T-matrix approach for this particular model of a porous medium with a single set of cracks, where the aspect ratio of the correlation function is identical with that of the cracks (figure 9). The reason for this is that the interactions cancel for this particular spatial distribution (see Ponte Castaneda and Willis 1995).

Hu and McMechan (2009) performed a small numerical experiment to investigate which method is more physical. In this experiment the aspect ratio of cracks and crack distribution was set equal to 1, which represents an isotropic medium (the cracks degenerate to spherical pores). At ''crack'' density 0.24, the crack porosity will be equal to 100%, so there will be no solid rock, and, theoretically all stiffnesses must be zero (Hu and McMechan 2009). Only higher order T-matrix was able to correctly predict the zero effective stiffness at 100% porosity (see figure 10). Thus prediction of higher order T-matrix approach makes much more physical sense.

For the effects of fluid saturation on the effective properties of a fractured and composite porous media, I have used anisotropic Gassmann relations of Brown and Korringa (1975). In case of a fractured/composite porous medium which is partially saturated with different fluids (oil, gas and water), the bulk modulus of the fluid may be regarded as the bulk modulus of an effective fluid and I have used the well known relation of Wood (Wood 1955).
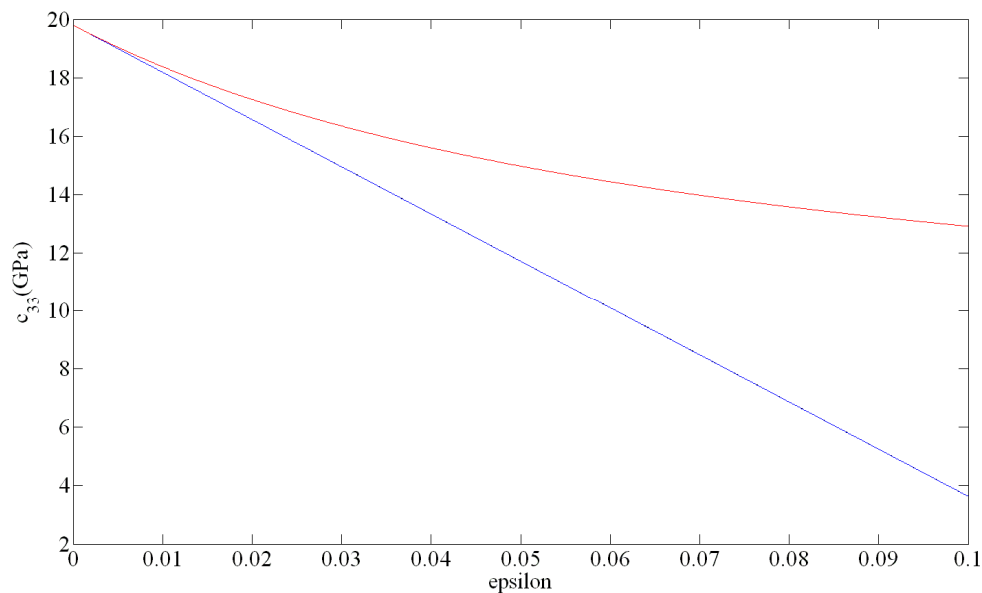
Figure 8 Comparison of dry effective stiffness constant c_{33} to the first order in crack density (epsilon) obtained using T-matrix approach (blue line), Hudson's model (black line) and NIA approach (red line). T-matrix and Hudson's model give exactly the same. The aspect ratio of cracks is 1/1000.
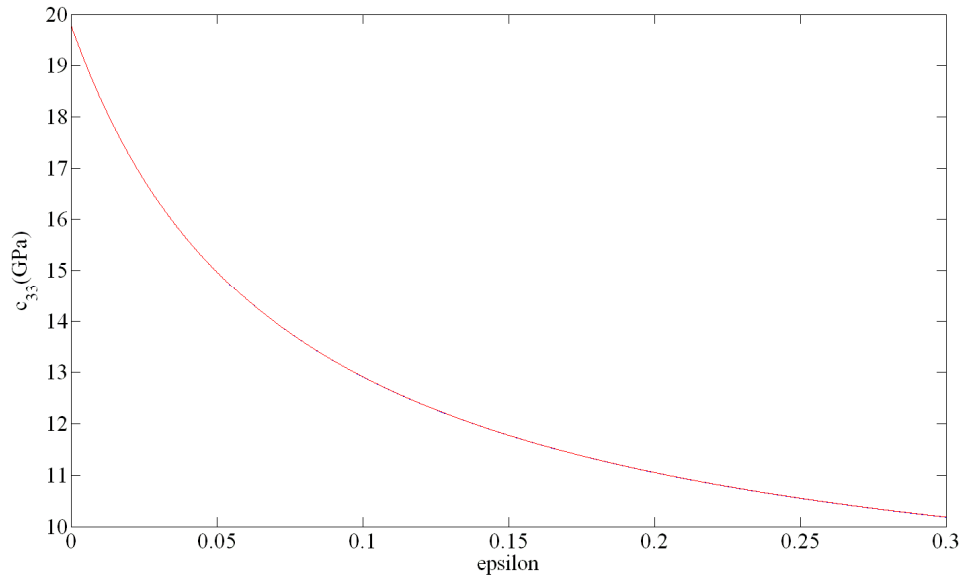
Figure 9 Comparison of dry effective stiffness constant c_{33} as a function of crack density (epsilon) obtained using higher order T-matrix approach (blue line) and NIA approach (red line). Both the approaches give exactly the same. The aspect ratio of cracks is 1/1000.
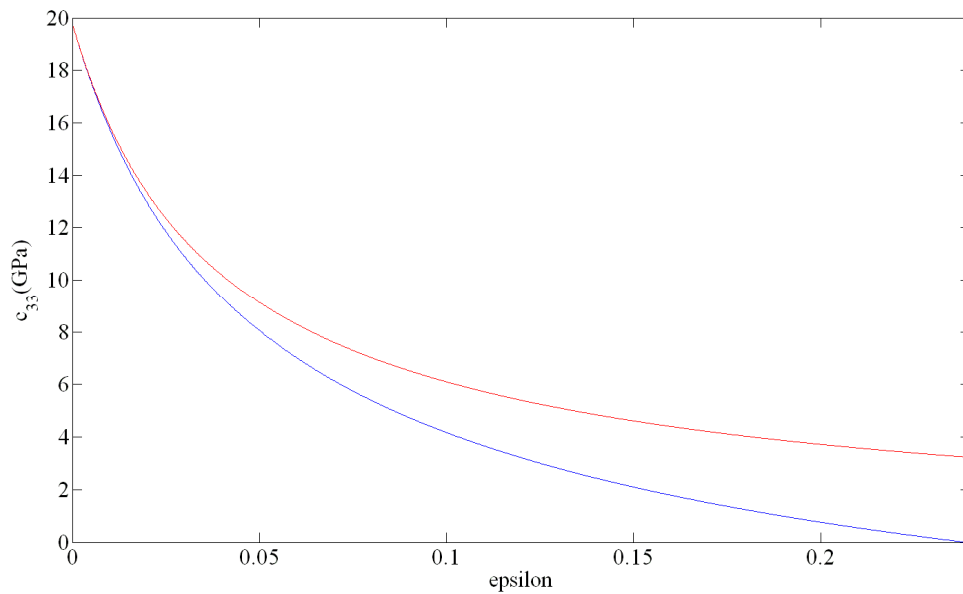
Figure 10 Predictions for dry effective stiffness constant c_{33} using higher order T-matrix approach (blue) and NIA method (red) for a model in which cracks degenerate to spherical pores by setting the aspect ratio of cracks and crack distribution equal to 1.

4.2 Seismic modelling

Seismic modelling is the next important step in the seismic fracture characterization, which is performed after obtaining the saturated effective elastic or viscoelastic properties of the fractured and composite porous media. Variations in elastic properties of rocks caused by fractures are detectable in certain special seismic attributes such as variation of amplitude with azimuth, shear-wave birefringence and azimuthal variation of propagation velocity for the fractured interval (Crampin et al., 1980; Lynn et al., 1995: Lynn et al., 1999; Zhu et al., 2004; Will et al., 2005). The purpose of seismic modelling in this thesis was to obtain attributes which are sensitive to the presence of aligned inclusions (fractures or deformation bands). More specifically, I have used the azimuthal variation of reflection coefficients or interval velocity and attenuation data. To obtain the seismic AVAZ data (reflection coefficients as function of polar angle of incidence and azimuth) in anisotropic media (HTI or monoclinic symmetry), I have used Rüger's approximation (Rüger, 1998; Ruger, 2002) and exact relations of Zoeppritz generalized to anisotropy (Schoenberg and Protazio, 1992).

The purpose of seismic modelling is to obtain the synthetic seismograms and/or special seismic attributes. The synthetic seismograms can be processed in the same manner as the real seismic data and compared with the observed seismic data. The comparison between observed and predicted seismic data can be done at various stages of seismic processing; that is, one can compare waveforms, amplitudes or acoustic impedances. In what follows, I present a brief review of the most commonly used computational methods for synthetic seismograms, such as ray theory and the finite difference method.

The fundamental concept in the seismic modelling is to solve the equation of motion for seismic waves. Ray theory is a well known method, which is used to compute seismic travel times and amplitudes along ray paths in a heterogeneous medium involving the high frequency approximation (Krebes, 2004). The travel time T of the

wave from source to a point **x** in a heterogeneous isotropic medium can be found by Eikonal equation given by (Krebes, 2004)

$$(\nabla T)^2 = \left(\frac{\partial T}{\partial x}\right)^2 + \left(\frac{\partial T}{\partial y}\right)^2 + \left(\frac{\partial T}{\partial z}\right)^2 = \frac{1}{v^2}, \tag{1}$$

where v is the seismic wave speed at the point **x**. Once T is known, the ray amplitude (A) can be computed in the high frequency approximation, by solving the transport equation for the wave and for the simple case of an acoustic wave is given by (Krebes, 2004)

$$2\nabla A \cdot \nabla T + A \nabla^2 T = 0. \tag{2}$$

For tracing the rays through a medium, a thorough discussion about different methods including the dynamic ray tracing for complex subsurface structures is presented by Cerveny (2001).

To obtain the synthetic seismograms using ray theory, I consider a simple model consisting of a stack of flat homogenous layers (figure 11) in which the reservoir layer is anisotropic (vertically aligned fractures). I have followed Krebes (2004), who presented simple algebraic formulas to compute the travel times and amplitudes of the rays for a medium consisting of a stack of flat homogenous isotropic horizontal layers. The only difference was at the top boundary of the reservoir, where I have used Rüger's approximation (Rüger, 1998; Ruger, 2002) to obtain the anisotropic reflection coefficients in HTI media. Once the travel times and amplitudes of the rays are computed, I have used the convolution method (Krebes, 2004; Sen, 2006) to generate the synthetic seismograms. Figure 12 show the synthetic seismograms just for illustration purposes for an azimuth of 45° for this particular model (figure 11).
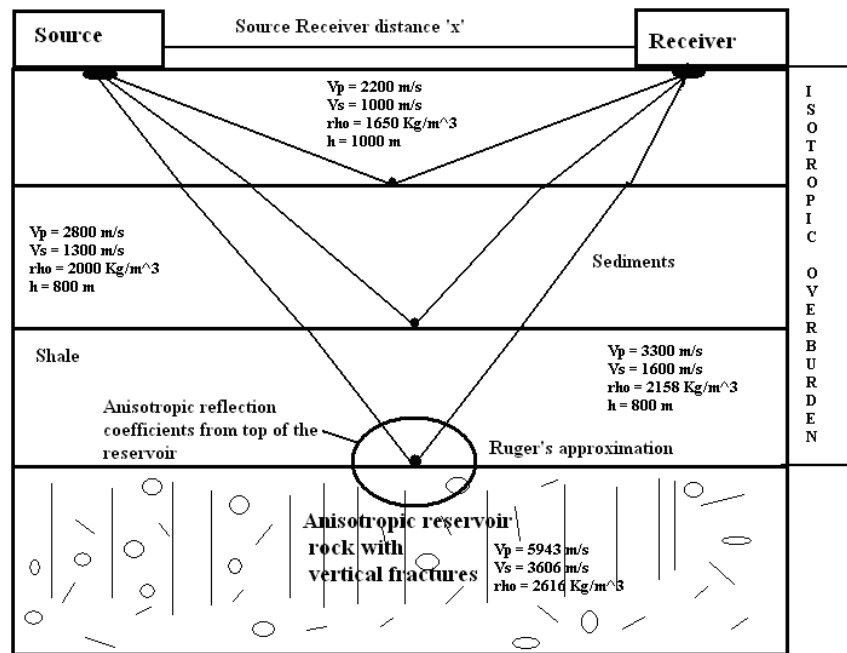
Figure 11 A simple seismic model consisting of stack of layers with isotropic shale layer overlying an anisotropic (fractured) reservoir, used in connection with a combination of ray theory and convolution method for seismic modelling. The P-wave, S-wave, density and thickness of each layer is also given.
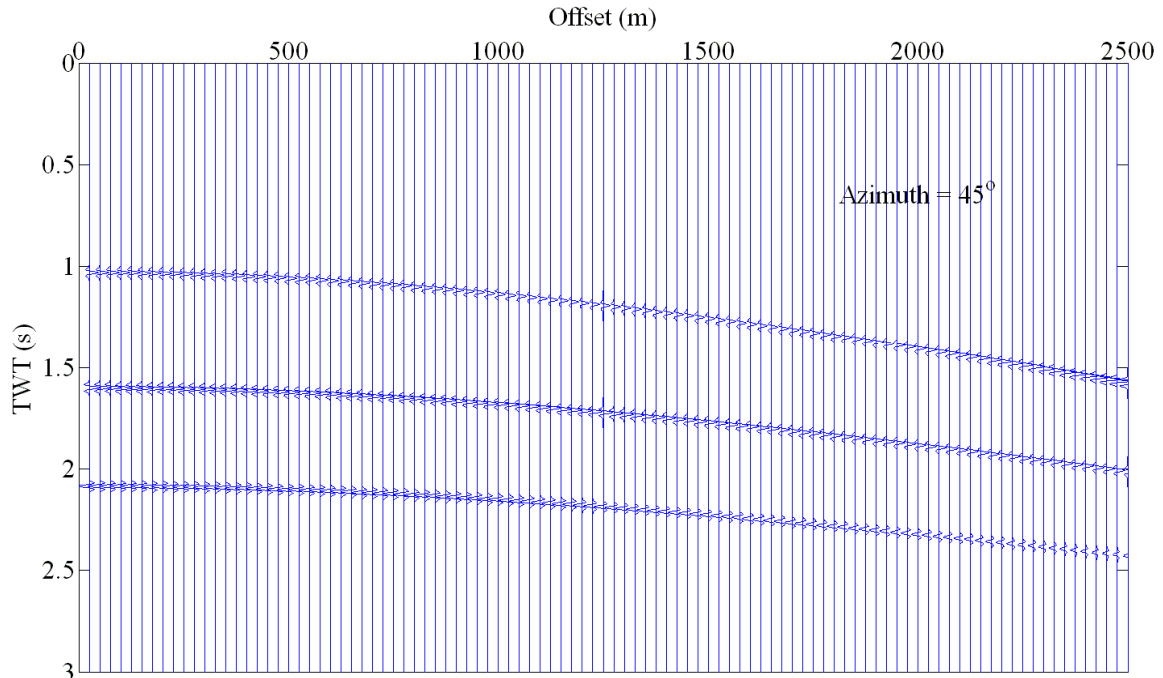
Figure 12 Synthetic P-wave seismograms generated by using a combination of ray theory and convolution method for a seismic model given in figure 11. A Ricker wavelet of 25 Hz frequency is used for the generation of source wavelet.

Finite difference (FD) method is the other important and most popular method for generating synthetic seismograms by solving partial differential equations. It uses a grid and compute the waveform in each sub-grid by approximating the values of derivatives occurring in the equation of motion by finite difference formulas and then solving the resulting equation recursively. For approximating the values of derivatives, one can use forward-difference approximation, backward-difference approximation or the central-difference approximation (Krebes, 2004). To increase the accuracy one must use smaller grid sizes, and to avoid grid dispersion, one can use the size of the grids of the order of dominant wavelength in the wave field. A problem of FD method is the generation of artificial reflection from the edges of the numerical grid, which can be resolved by the use of absorbing or non-reflecting conditions (Krebes, 2004). The finite difference calculations can also be very time consuming.

In order to obtain the reflection coefficients as a function of polar angle of incidence and azimuth from seismic waveforms, prestack migration data should be available. This analysis requires carefully designed acquisition geometries and a careful selection of applied processing algorithms. For example, sophisticated processing routines such as deconvolution, amplitude preserving migration and Q compensation (compensation for intrinsic attenuation) are required.

4.3 Bayesian inversion

4.3.1 General considerations

The goal of inverse modelling is to estimate the parameters related to fractures or deformation bands, which control the fluid flow during production. In this PhD thesis, I have used Bayesian approach for solving the inverse problem in the context of seismic characterization of fractured reservoirs. The classical approach to the inverse problems assumes that there exists a specific but unknown model $\mathbf{m}$ needed to be discovered (Aster et al., 2005). The Bayesian approach to the inverse problems assumes the true model $\mathbf{m}$ as a random variable and the solution is a probability distribution for the model parameters (Aster et al., 2005). One of the advantages of the Bayesian approach is that it allows incorporating a priori information collected independently from the measurements.

I formulate my inverse problem given by

$$\mathbf{G}(\mathbf{m}) \approx \mathbf{d}. \tag{3}$$

Here, $\mathbf{m}$ is a vector of model parameters related with fractures and/or deformation bands and $\mathbf{d}$ is a vector of observable quantities (seismic AVAZ data). $\mathbf{G}$ is a combination of rock physics modelling discussed in section 4.1 and the seismic modelling discussed in section 4.2. The solution of an inverse problem in a Bayesian setting is given by the posterior probability $q(\mathbf{m}|\mathbf{d})$ distribution over the model space M. The posterior probability distribution and $q(\mathbf{m}|\mathbf{d})$ and prior distribution $p(\mathbf{m})$ are related with each other in a way that makes the computation of posterior possible given by Baye's theorem (Aster et al., 2005)

$$q(\mathbf{m}|\mathbf{d}) \propto f(\mathbf{d}|\mathbf{m}) p(\mathbf{m}), \tag{4}$$

where the likelihood function and prior distribution are given by

$$f(\mathbf{d}|\mathbf{m}) \propto \exp\left[-\frac{1}{2}(\mathbf{G}(\mathbf{m})-\mathbf{d})^T \mathbf{C}_D^{-1}(\mathbf{G}(\mathbf{m})-\mathbf{d})\right],$$

$$p(\mathbf{m}) \propto \exp\left[-\frac{1}{2}(\mathbf{m}-\mathbf{m}_0)^T \mathbf{C}_D^{-1}(\mathbf{m}-\mathbf{m}_0)\right],$$

(5)

where $\mathbf{m}_0$ is defined as the expected value of the a priori distribution. Then the posterior distribution function can be defined as (Aster et al., 2005)

$$q(\mathbf{m}|\mathbf{d}) \propto N \cdot e^{-J(\mathbf{m})},$$

(6)

where N is a constant and $J(\mathbf{m})$ is the objective or cost function and for Gaussian statistics given by (Aster et al., 2005)

$$J(\mathbf{m}) = \frac{1}{2}\left[(\mathbf{G}(\mathbf{m})-\mathbf{d})^T \mathbf{C}_D^{-1}(\mathbf{G}(\mathbf{m})-\mathbf{d}) + (\mathbf{m}-\mathbf{m}_0)^T \mathbf{C}_M^{-1}(\mathbf{m}-\mathbf{m}_0)\right].$$

(7)

Here, $\mathbf{C}_D$ and $\mathbf{C}_M$ are the covariance matrices for the data and for the model respectively. The posterior PDF represents the degrees of belief about the possible values of $\mathbf{m}$ before and observing the data $\mathbf{d}$. If we have uninformative prior, then this equation (7) reduces to

$$J(\mathbf{m}) = \frac{1}{2}\left[(\mathbf{G}(\mathbf{m})-\mathbf{d})^T \mathbf{C}_D^{-1}(\mathbf{G}(\mathbf{m})-\mathbf{d})\right].$$

(8)

The constant N in equation (6) can be found by integration. Assume that the model parameters $\mathbf{m}$ are defined in the model space M i.e. $m \in M$, then the posterior distribution will satisfy (Aster et al., 2005)

$$\int_M q(\mathbf{m}|\mathbf{d})d\mathbf{m} = 1 \Rightarrow N = \frac{1}{\int_M e^{-J(\mathbf{m})}d\mathbf{m}}.$$

(9)

The inverse problem using the seismic AVAZ data is ill-conditioned and sometimes ill-posed, raising questions about the reliability of the estimates (Downton et al., 2007). So it is very important to perform the uncertainty analysis of the predicted estimates. To quantify the prediction uncertainty in the estimates of model parameters,

an assessment of the full posterior distribution $q(\mathbf{m}|\mathbf{d})$ is required. Since the forward modelling in this study is highly nonlinear and cannot be expressed by a simple formula, an analytical evaluation will be prohibited and the exploration of the posterior probability density function (PDF) can only be done by sampling. Rejection sampling (Ross, 1997) and Monte Carlo Markov chain (MCMc) sampling (Sambridge and Mosegaard, 2002; Tarantola, 2005; Liu and Oliver, 2003;) are the two sampling routines that can be used to sample from posterior PDF. The problem with rejection sampling is that one needs to have an estimate of the posterior PDF in order to obtain a satisfactory acceptance (or rejection) rate, suggesting that the method is not very efficient. MCMc methods are very efficient in this respect, and only need relatively high number of samples in order to generate statistical histograms that resemble the true PDFs (Liu and Oliver, 2003).

To obtain the marginal PDFs I have used MCMc method (in paper 2, 3, 5 and 6). In paper 1, I have used numerical integration method, which yields the marginal PDFs for small dimensional problems (Tarantola, 2005). Also in paper 1, when inverting for a distribution of model parameters (analysis of more than one grid blocks), the minimum/maximum of the objective function given in equation (7) is obtained via a systematic search through all allowed points within a discretized version of the model parameters (Tarantola, 2005). The problem of finding the minimum of the objective or cost function is the same as finding the maximum of the posterior distribution. In what follows, I present a very brief introduction about finding the marginal PDFs using numerical integration and MCMc methods. A comparison of marginal PDFs obtained via numerical integration and MCMc methods is also presented for a simple case where I have two unknown model parameters related with fractures (fracture density and azimuthal fracture orientation).

4.3.2 Marginal PDFs via numerical integration and MCMc method

The marginal PDFs of the model parameters can be found by integrating the model parameters with respect to other model parameters. For example, I consider the case

when I have two unknown model parameters (fracture density and azimuthal fracture orientation) in the context of fracture characterization. The marginal PDFs for the fracture density and the azimuthal fracture orientation can be obtained in the following way.

Let ε denote the fracture density, ψ denote the azimuthal fracture orientation and M is the model space for the parameters, the posterior distribution satisfies (Equation (9))

$$\int_0^\pi \int_0^{\varepsilon_{max}} q(\varepsilon, \psi) d\varepsilon d\psi = 1. \tag{10}$$

The marginal distribution for the fracture density will then be obtained by integrating over all the azimuthal fracture orientations i.e.

$$q_\varepsilon(\varepsilon) = \int_0^\pi q(\varepsilon, \psi) d\psi. \tag{11}$$

Similarly, the marginal distribution for azimuthal fracture orientation can be obtained by integrating over all the fracture densities i.e.

$$q_\psi(\psi) = \int_0^{\varepsilon_{max}} q(\varepsilon, \psi) d\varepsilon. \tag{12}$$

Marginal PDFs obtained via numerical integration require dense discretization of the model space. Sparse discretization of model space may lead to missing of important features of posterior distribution. This method is only useful when the computation of forward model is not much time consuming and we have a small dimensional problem at our hand. For high dimensional problems and time consuming forward problem, this method might proves to be ineffective.

To obtain the marginal PDFs using MCMc method, I have used the Metropolis algorithm (Metropolis and Ulam, 1949; Metropolis et al., 1953; Hastings 1970; Tarantola, 2005) to generate independent samples from the posterior PDF. The

method is random (Monte Carlo) and has no memory, as each step depends only on the previous step (Markov chain). A random walk is performed which obtains samples from the initial probability distribution, then by the application of some probabilistic rules the random walk is modified, so that the modified random walk samples the target distribution (Tarantola, 2005). An important thing to note is that there is no general rule for obtaining the independent posterior samples, as this strongly depends on the particular problem at hand. The efficiency of the algorithm is determined by the acceptance rate. The random walk should be designed in a sense that the perturbations of the likelihood function is as small as possible as this will increase the acceptance rate of the Metropolis rule (Tarantola, 2005). The perturbation size in the model space should be such that the acceptance rate of the Metropolis criterion is 30-50% (Tarantola, 2005). If the acceptance rate is larger, we are not moving fast enough in the model space; if it is smaller, we are wasting our resources to test models that are not accepted (Tarantola 2005).

Figure 13 show the comparison of marginal PDFs obtained via MCMc and numerical integration methods for a small dimensional problem of two unknown model parameters (fracture density and azimuthal fracture orientation). A combination of the T-matrix approach of Jakobsen et al., (2003a) with the anisotropic Gassmann relations of Brown and Korringa (1975) is used to relate the parameters of fractures to the effective undrained elastic constants. Rüger's approximation (Rüger, 1998, 2002) is used to obtain the reflection coefficients as a function of polar incidence and azimuthal angles from top of the reservoir. The properties of solid mineral, dry porous matrix, fluid and overburden used for the numerical calculations are given in table 1. The true fracture density and azimuthal fracture orientation is set to 0.05 and 35°.

Material	Bulk modulus (GPa)	Shear Modulus (GPa)	Density (kg/ m³)
Dry porous matrix (Carbonate)	41.2	25.2	2500
Solid Mineral (Calcite)	72.0	45.0	2710
Fluid (Brine)	2.2	0.0	1000
Isotropic Overburden	44.5	25.4	2633

Table 1 The properties of dry porous matrix (Nolen-Hoksema et al., (1995)), solid mineral, fluid and isotropic overburden used to perform numerical calculations in figure 13.
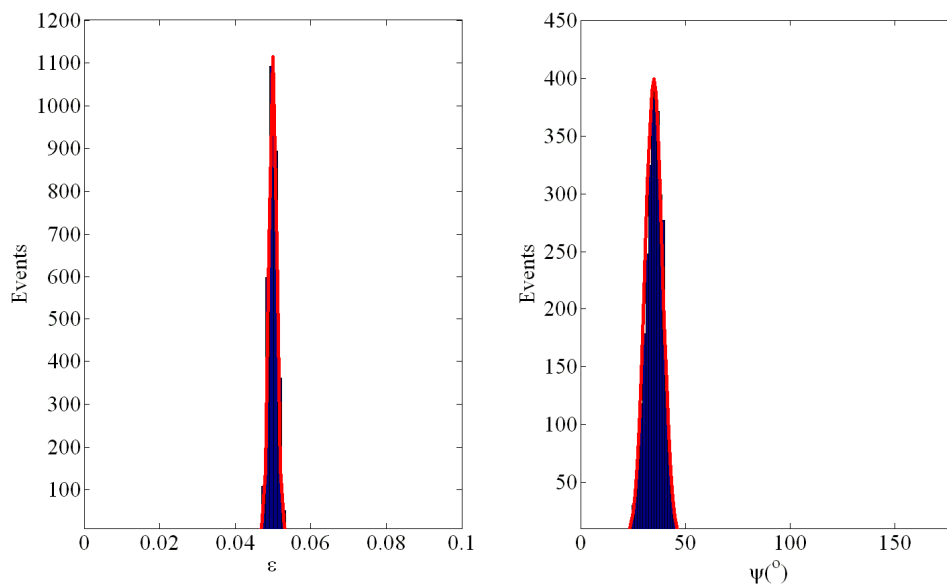

Figure 13 Comparison of marginal PDFs obtained via MCMc (blue bars) and numerical integration (red line) methods. The standard deviation of the measured seismic data was set to 20% and an uninformative prior was considered during the inversion.

5. Main scientific contributions

The main scientific contributions of the thesis consist of a set of research papers describing the development of novel workflows about the correlations between effective permeability and seismic anisotropy of fractured and composite porous media. In this section, I present each of the papers with their objectives and relevance, and their main findings and conclusions are summarized. The full length papers are presented in Part II. The appendices of part II consist of corresponding extended abstracts for papers 1, 2, 3, 4 and 6. The ideas and methodology presented in extended abstracts has been extended leading to papers described above.

Paper 1: On the accuracy of Rüger's approximation for reflection coefficients in HTI media: Implications for the determination of fracture density and orientation from seismic AVAZ data

Reflection coefficients as a function of offset and azimuth are mostly used as an important seismic attribute when dealing with the characterization of fractured reservoirs. The added dimension of azimuth in anisotropic media makes the reflection problem more challenging. To cope up with this challenge, several approximate forms for the reflection problem in anisotropic media have been introduced. Among these approximate forms, the most popular and widely used in the industry is Rüger's approximation for a medium with horizontal axis of symmetry (Rüger 1998, Rüger 2002). The main reason for its wide use is that the effect of anisotropy on reflection signature can be analyzed with the help of a simple analytic approximation and it gives direct and straightforward insight into the azimuthal signature. In this paper, we have investigated the accuracy of Rüger's approximation for PP reflection coefficients in HTI media relative to an exact generalization of Zoeppritz to anisotropy derived by Schoenberg and Protazio (1992) within the context of seismic fracture characterization.

More specifically, we investigate the implications of Rüger's approximation for the determination of fracture density and azimuthal orientation, as well as the accuracy in forward modelling of reflection coefficients. A combination of the T-matrix approach of Jakobsen et al., (2003a) with the anisotropic Gassmann relations of Brown and Korringa (1975) is used to relate the parameters of the fractures to the effective (undrained) elastic constants. The inversion of this non-linear forward model was done in a Bayesian setting, which provides information about uncertainties as well as the most likely values. The main outcomes of this study are:

- Rüger's approximation can be used to recover the fracture density with small uncertainty if and only if the fracture density and contrast is significantly smaller than the values that is believed to occur in many practically interesting cases of fractured (carbonate) reservoirs.

- Rüger's approximation can be used to obtain estimates of the azimuthal fracture orientation with small uncertainty, even when the contrast and anisotropy level is extremely large.

- It is generally safer and not extremely more computationally expensive to use the exact generalization of Zoeppritz to anisotropy provided by Schoenberg and Protazio (1992) rather than Rüger's approximation; but Rüger's approximation seems to give the estimates of the fracture orientation with small uncertainty, and it can sometimes give (fit for purpose) qualitative information about the trends in the spatial distribution of the fractures.

Paper 2: Improved characterization of fault zones by quantitative integration of seismic and production data

The impact of faults on the flow of fluids in hydrocarbon reservoirs has been recognized long time ago. In reality, faults are complex 3D objects typically consisting of fault core surrounded by a heterogeneous damage zone. The fault

damaged zone typically consists of fractures or deformation bands that may or may not have a preferred orientation. The purpose of this paper was to obtain an improved characterization of fault zones by quantitative integration of seismic AVAZ and production data. Our workflow is based on a consistent stiffness-permeability model for the fractured or composite porous media in the damage zone, and a Bayesian (Monte Carlo Markov chain) method of inversion, which provides information about uncertainties as well as the most likely values of the model parameters. We have generated synthetic seismic and production data for a model of a fault zone, and demonstrated how accurately one can recover the fault core transmissibility and the parameters of the fault damaged zone from production and seismic amplitude versus angle-azimuth (AVAZ) data that have been contaminated with random noise. This study represents an extension of the fracture characterization system developed by Jakobsen et al., (2007a, b) and Jakobsen and Shahraini (2008a, b) in the sense that we have introduced the fault core as an additional complication, that increases the non-uniqueness associated with the inverse problem. The main outcomes of this study are:

- The study shows that seismic and production data are complementary to each other. The reason is that seismic data are sensitive to the fault transmissibility via saturation but the effects were not large enough, so that the seismic data alone can recover the fault transmissibility.

- The joint inversion of seismic and production data also helps to reduce the uncertainty in the fault transmissibility along with fracture density or volume fraction of deformation bands.

This paper is published online in Journal of Geophysics and Engineering. There is some confusion with figures 4, 5, 6 and 7 in the paper related with the axis of 3D-plots. For example, in figure 4 it shows increasing stiffness with increasing fracture density. The figures are not wrong, only the axis must be reversed. For this purpose, the figures 14, 15, 16 and 17 with correct axis are shown here.
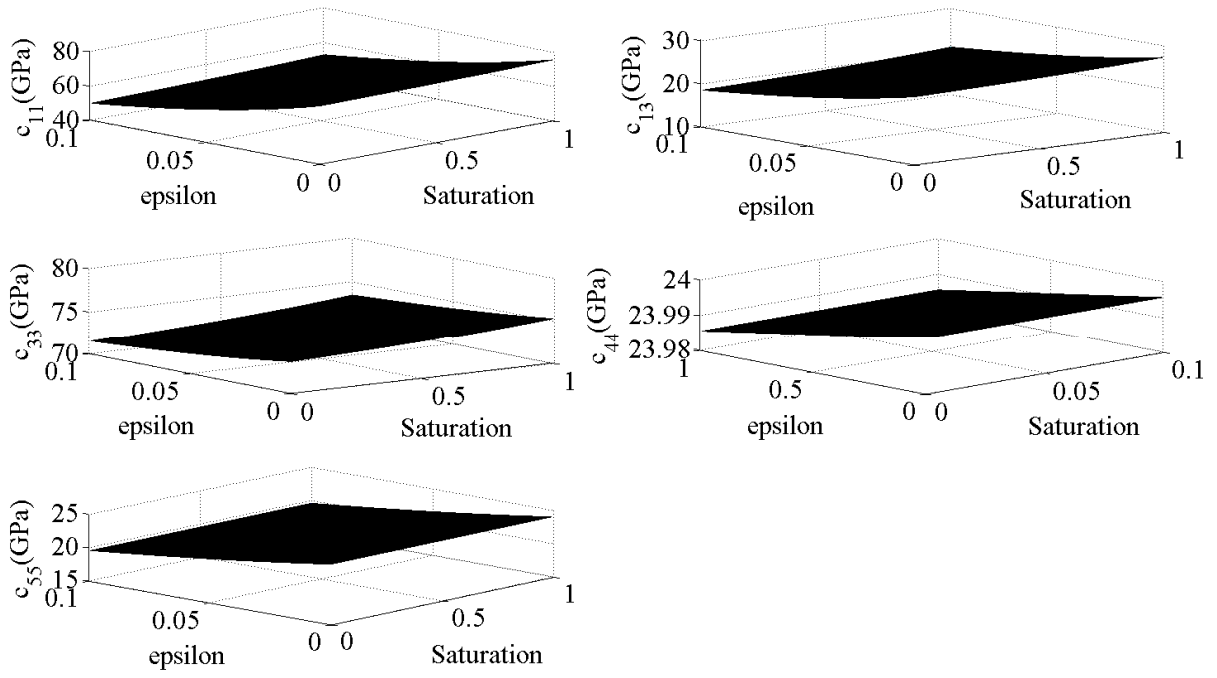
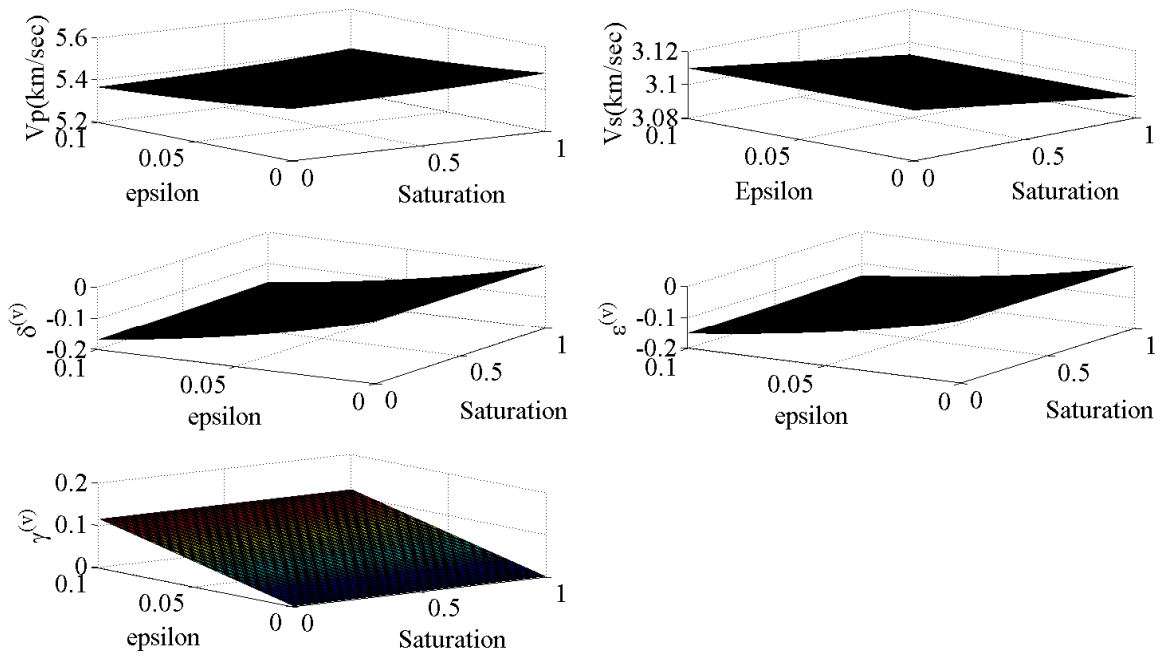*Figure 14 Axis-corrected version of the figure 4 in paper 2.*

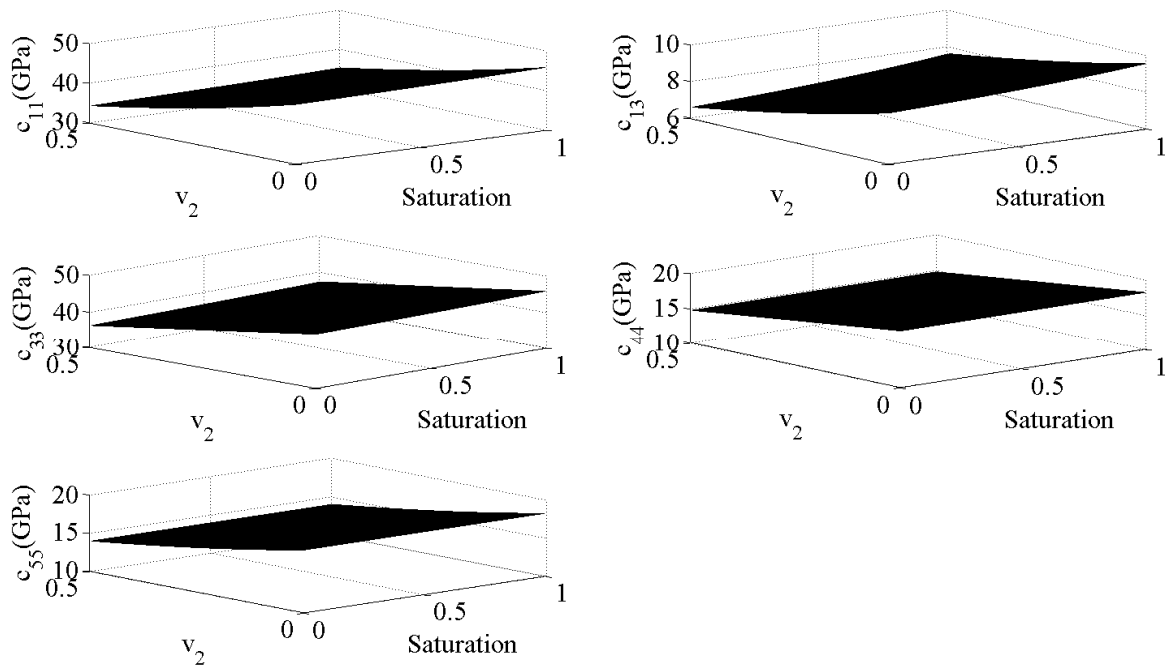*Figure 15 Axis-corrected version of the figure 5 in paper 2.*

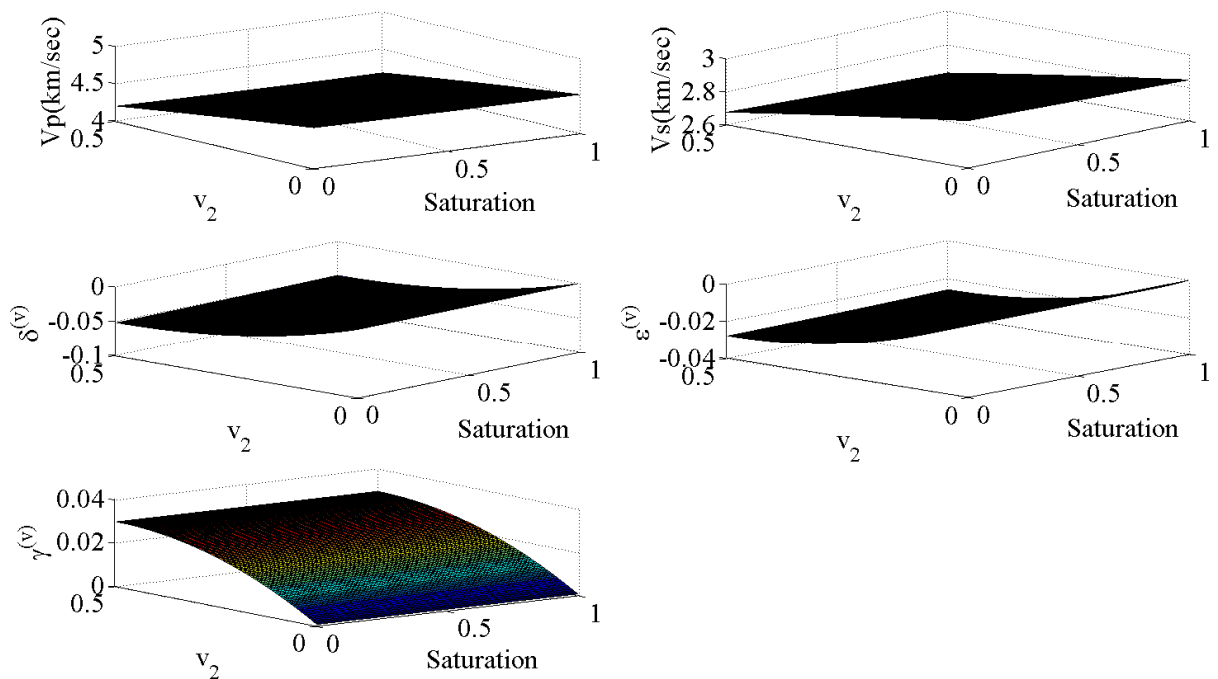*Figure 16 Axis-corrected version of the figure 6 in paper 2.*

Figure 17 Axis-corrected version of the figure 7 in paper 2.

Paper 3: Characterization of fractured reservoirs using a consistent stiffness-permeability model: focus on the effects of fracture aperture

This paper proposes a method for the characterization of naturally fractured reservoirs by quantitative integration of seismic and production data. Previous studies (Jakobsen et al., 2007a) showed that there is a high uncertainty in the estimated effective permeability using only seismic AVAZ data due to the low sensitivity of the effective stiffness tensor to the aperture. In this paper, we have inverted for all the three fracture parameters (e.g., fracture density, orientation and aperture) that determine the effective permeability tensor of a fractured reservoir. The method is based on a consistent theoretical frame work to model both effective hydraulic and elastic properties of fractured porous media and a (non-linear) Bayesian method of inversion that provides information about uncertainties as well as mean (or maximum likelihood) values. We model a fractured reservoir as a porous medium containing a single set of vertical fractures characterized by an unknown fracture density, azimuthal orientation and aperture. We then look at the problem of fracture parameter estimation as a non-linear inverse problem and try to estimate the unknown fracture parameters by joint inversion of seismic AVAZ data and dynamic production data. Once the fracture parameters have been estimated the corresponding effective stiffness and permeability tensors can be estimated using consistent models. The main outcome of this study is:

- This study shows that seismic and production data complement each other, in the sense that the seismic data resolve non-uniqueness associated with fracture parameters (fracture density and orientation) and the production data help to recover the fracture aperture and the effective permeability tensor, because production data are more sensitive to the fracture aperture than the seismic data.

Paper 4: On the relative importance of global and squirt flow in cracked porous media

An important aspect of this PhD project was to investigate the phenomenon of wave induced fluid flow to develop new methods for improved reservoir simulations by seismically derived fractured models. This requires developing new workflows for the estimation of anisotropic permeability in fractured reservoirs from measurements of frequency-dependent seismic anisotropy attributes. For this purpose, we have first investigated the relative importance of global and squirt flow in cracked porous media using the unified theory of Jakobsen and Chapman (2009). More specifically, we have investigated the implications of unified theory of Jakobsen and Chapman (2009) for the relative importance of global and squirt flow characterized by different microstructures and fluid mobilities. A further aim was to investigate if a prediction of negative velocity dispersion in certain models where global flow dominates will change significantly if one accounts for certain effects of non-local elasticity that exists in the unified theory (Jakobsen and Chapman, 2009), but have never been implemented in a proper manner. We use an iterative method for solving the nonlinear equations associated with the unified theory of global and squirt flow in cracked porous media, where the effective stiffness tensor depends on the frequency and effective wave vector. A quadratic equation representing microstructural and phenomenological theories of wave-induced fluid flow in isotropic media to the first order in porosity or crack density is also presented. We also present and apply a simple model for the effects of viscosity on the relaxation time constant for squirt flow associated a particular pore/shape orientation. The main outcomes of this study are:

- The magnitude of squirt flow dominates over global flow and global flow appears to be important at higher frequencies for more realistic microstructures (models like pores and randomly oriented micro-cracks or pores, randomly oriented micro-cracks and aligned mesoscopic fractures).

- The attenuation peak of squirt flow move towards relatively low frequencies with the increase of viscosity i.e. changing saturating fluid from water to oil, while the global flow attenuation peak move towards relatively high frequencies with the increase of viscosity.

- The attenuation peak of the global flow obtained using the approximate wave number is always shifted to the right as compared to the solution with correct wave number (exact analytical or iterative solution).

- This study shows that the observations of negative velocity dispersion in Jakobsen and Chapman (2009) theory still remain, even if we use the correct effective wave number, when dealing with the phenomenon of wave-induced fluid flow in models of cracked /fractured porous media where global flow effects dominates.

- At seismic frequencies global flow effects are not so important and needs high permeability and low viscosity to have an effect.

Paper 5: Anisotropic permeability in fractured reservoirs from frequency-dependent seismic AVAZ data

Attempts to predict permeability from seismic AVAZ data on the basis of a combination of the consistent stiffness-permeability model with the anisotropic Gassmann relations of Brown and Korringa are not very much successful due to the low sensitivity of effective stiffness to fracture aperture than the corresponding effective permeability tensor (Jakobsen et al., 2007a). The presence of mesoscopic fractures in a reservoir can produce significant dispersion and attenuation at seismic frequencies, suggesting that it is generally not safe to treat seismic frequencies as the low frequency limit (Maultzsch *et al*. 2003). In this paper, we show that one can obtain information about all the three fracture parameters that determines the effective permeability tensor (that is, the fracture aperture as well as the fracture density and orientation), provided that the anisotropic Gassmann relations are replaced by a theory

for seismic attenuation and dispersion due to wave-induced fluid flow; and the reflection coefficients are no longer assumed to be real-valued and frequency-independent. Synthetic seismic AVAZ data are generated by using a combination of a dynamic effective medium theory with Rüger's approximations for PP reflection coefficients in HTI media. A Monte Carlo method is used to perform a Bayesian inversion of these synthetic seismic AVAZ data with respect to the parameters of the fractures. The effective permeability model is then used to construct the corresponding probability density functions for the different components of the effective permeability constants. The main outcome of this study is:

- Improved estimation of anisotropic permeability can be obtained via frequency-dependent seismic AVAZ data i.e. including the velocity dispersion and attenuation associated with mesoscopic fractures using a dynamic effective medium theory.

Paper 6: Seismic characterization of reservoirs with multiple fracture sets using velocity and attenuation anisotropy data

The workflow described in paper 5 can be extended to more complex fractured reservoir characterization i.e. a fractured reservoir with multiple sets of fractures. This is also due to the fact that T-matrix part of the workflow described in Paper 5 represents the most general model, because it allows for non-dilute concentrations of inclusions characterized by different shapes, orientations and spatial distributions (Gurevich et al., 2009; Müller *et al*. 2010). In this paper, we use measurements of velocity and attenuation anisotropy data corresponding to different seismic frequencies and azimuths to infer important information about the multiple fracture sets present in the reservoir. We model a reservoir containing two sets of vertical fractures characterized by unknown azimuthal fracture orientations and fracture densities. Synthetic seismic velocity and attenuation anisotropy data is computed using effective viscoelastic stiffness tensor solving the Christoffel equation. A Bayesian inversion method is then applied to measurements of velocity and

attenuation anisotropy data corresponding to different seismic frequencies and azimuth to estimate the azimuthal fracture orientations and the fracture densities, as well as their uncertainties. The main outcomes of this study are:

- For fractured reservoir containing two sets of aligned mesoscopic fractures, one can in principle estimate the azimuthal fracture orientations and fracture densities from measurements of seismic velocity and attenuation anisotropy data corresponding to different seismic frequencies and azimuths, provided that one has priori information about the porous matrix, saturating fluid(s) and fracture geometry.

- Measurements of velocity anisotropy data alone corresponding to different seismic frequencies and azimuths cannot recover the fracture parameters related with multiple sets.

- A satisfactory characterization of complex fractured reservoirs requires a model accounting for attenuation anisotropy.

6. Concluding remarks and possible extensions

This study contains novel workflows and methodologies to exploit the correlations between effective permeability and seismic anisotropy of fractured reservoirs. The workflows and methodologies are based on the rock physics models that calculate the effective mechanical and transport properties of the fractured and composite porous media. Bayesian approach has been used to solve the non-linear inverse problem of finding the parameters related with fractures from seismic amplitude versus angle and azimuth (AVAZ) data (frequency-independent or frequency-dependent) and/or production data. This study shows that improved characterization of fractured or composite porous media can be obtained either using the joint inversion of frequency-independent seismic AVAZ data and production data or the frequency-dependent seismic AVAZ data obtained by including the seismic velocity dispersion and attenuation data.

This study can be extended in multiple directions. An obvious extension is the use of seismic AVAZ data obtained from the synthetic seismograms by the application of proper processing routines as for real seismic data instead of using the amplitude of the reflection coefficients from the top of the reservoir. In this way the effect of the overburden can also be incorporated in a proper manner. The synthetic seismograms can be obtained via ray theory or finite difference methods (see Krebes, 2004). Seismic AVAZ data obtained in this manner can then be used in Bayesian inversion methodology to obtain the parameters related with fractured and composite porous media and the corresponding effective permeability estimates.

Another possible extension of the workflow can be performed by involving other data types e.g., shear wave birefringence. The shear wave birefringence is often taken as proportional to the fracture density in the case of single set of aligned fractures. Shear wave birefringence also tends to be quite robust, so incorporation of such type of data can improve the efficiency of the proposed methodology.

A further extension can be to include the effects of percolation in the rock physics models. In this study we have considered that the fractures are isolated with respect to fluid flow, but for the effects of intersecting fractures, the percolation effects should be included. A self-consistent approach can be used to model the effect of interconnected fractures (Pozdniakov and Tsgang, 2002).

Another improvement in the workflow can be obtained by performing the joint inversion of frequency-dependent seismic AVAZ data and production data for improved characterization of reservoirs with complex fracture system i.e. multiple sets of fractures.

A further improvement in the method can be to include the effects of pressure in the rock physics models. Fracture aperture is the most important parameter controlling the fluid flow and pressure changes can have an important affect on the aperture of the fractures.

References

Agersborg, R., Jakobsen, M., Ruud, B.O., & Johansen, T.A. (2007): Effects of pore fluid pressure on the seismic response of a fractured carbonate reservoir, Studia Geophysica et Geodaetica, 51, 89-118.

Aguilera, R. (1995): Naturally Fractured Reservoirs, PennWell Books, Tulsa, Olka.

Aster, R.C., Borchers, B. & Thurber, C.H. (2005): Parameter estimation and inverse problems, Elsevier Academic press, ISBN 0120656043.

Auld, B.A. (1990): Acosutic Fields and Waves in Solids, Krieger Publishing, Malabar, FL.

Brown, R.J.S. & Korringa, J. (1975): On the dependence of the elastic properties of a porous rock on the compressibility of the pore fluid, Geophysics, 40, 608-16.

Budiansky, B. & O'Connell, R.J. (1976): Elastic moduli of a cracked solid: International Journal of Solids and Structures, 12, 81–97.

Castañeda, P. & Willis, J.R. (1995): The effect of spatial distribution on the effective behavior of composite materials and cracked media, Journal of Mechanics and Physics of Solids, 43, 1919–51.

Červený, V. (2001): Seismic Ray Theory, Cambridge University Press, Cambridge.

Chapman, M. (2003): Frequency-dependent anisotropy due to meso-scale fractures in the presence of equant porosity, Geophysical Prospecting, 51, 369-79.

Chapman, M. (2009): Modeling the effect of multiple sets of mesoscale fractures in porous rock on frequency-dependent anisotropy, Geophysics, 74, D97-D103.

Cheng, C.H. (1993): Crack models for a transversely anisotropic medium, Journal of Geophysical Research, 98, 675-84.

Chopra, S., Chemingui N., and Miller R.D. (2005): An introduction to this special section - carbonates, The leading Edge, 24, 488-89.

Clark, R.A., Benson, P.M., Carter, A.J., and Guerrero Moreno, C.A. (2009): Anisotropic P-wave attenuation measured from a multi-azimuth surface seismic reflection survey, Geophysical Prospecting, 57, 835-45.

Crampin, S., McGonigle, R., & Bamford, D. (1980): Estimating crack parameters from observations of P-wave velocity anisotropy, Geophysics, 45, 345-60.

Downton, J., Gray, D., & Zuk T. (2007): Visualizing AVAZ parameter estimates and uncertainty, CSPG CSEG Covention, 256-59.

Eshelby, J.D. (1957): The determination of the elastic field of an ellipsoidal inclusion and related problems: Proceedings of the Royal soceity of London, Series, A, Mathematical and Physical sciences, 241, 376-96.

Fossen, H., Schultz, R.A., Mair, K., & Shipton, Z. (2007): Deformation bands in sandstones - A review: Journal of Geological Society (London), 164, 755-769, doi: 10.1144/0016-76492006-036.

Gray, D., Roberts, G., & Head, K. (2002): Recent advances in determination of fracture strike and crack density from P-wave seismic data, The Leading Edge, March 2002, 280-85.

Grechka, V. & Kachanov, M. (2006a): Effective elasticity of cracked rocks: A snapshot of the work in progress, Geophysics, 71, W45–W58.

Grechka, V. & Kachanov, M. (2006b): Effective elasticity of rocks with closely spaced and intersecting cracks, Geophysics, 71, D85–D91.

Grechka, V. & Kachanov, M. (2006c): Seismic characterization of multiple fracture sets: Does orthotropy suffice?, Geophysics, 71, D93–D105.

Gurevich, B., Brajanovski, M., Galvin, R.J., Müller, T.M., & Toms-Stewart, J. (2009): P-wave dispersion and attenuation in fractured and porous reservoirs – poroelasticity approach, Geophysical Prospecting, 57, 225-37.

Hastings, W.K. (1970): Monte Carlo sampling method using Markov chains and their applications, Biometrika, 57, 97-109.

Hoenig, A. (1979): Elastic moduli of a non-randomly cracked body, International Journal of Solids and Structures, 15, 137–54.

Hornby, B.E., Schwartz, L.M., & Hudson, J.A. (1994): Anisotropic effective-medium modeling of the elastic properties of shales, Geophysics, 59, 1570–83.

Hu, Y. & McMechan, G.A. (2009): Comparison of effective stiffness and compliance for characterizing cracked rocks, Geophysics, 74, D49-D55.

Hudson, J.A. (1980): Overall properties of a cracked solid: Mathematical Proceedings of the Cambridge Philosophical Society, 88, 371–84.

Hudson, J.A. (1981):Wave speeds and attenuation of elastic waves in material containing cracks: Geophysical Journal of the Royal Astronomical Society, 64, 133–50.

Hudson, J.A. (1994):Overall properties of a material with inclusions or cavities, Geophysical Journal International, 117, 555–61.

Hudson J.A., Liu E., & Crampin S. (1996): The mechanical properties of materials with interconnected cracks and pores, Geophysical Journal international, 124, 105-12.

Jakobsen, M., Hudson, J.A., & Johansen, T.A. (2003a): T-Matrix approach to shale acoustics, Geophysical Journal International, 154, 533–58.

Jakobsen, M., Johansen T.A., & McCann C. (2003b): The acoustic signature of fluid flow in complex porous media, Journal of applied Geophysics, 54, 219-46.

Jakobsen, M., and Hudson, J.A. (2003): Visco-elastic waves in rock-like composites, Studia Geophysica et Geodaetica, 47, 793-826.

Jakobsen, M. & Johansen, T. A. (2005): The effects of drained and undrained loading on visco-elastic waves in rock-like composites, International Journal of Solids and Structures, 42, 1597–1611.

Jakobsen, M., Liu E., & Chapman M. (2007a): Anisotropic permeability in fractured reservoirs from seismic AVOZ analysis, 77th SEG meeting, San Antonio, TX, USA, Expanded Abstracts.

Jakobsen, M., Skjervheim, J.A., & Aanonsen, S. (2007b): Characterization of fractured reservoirs by effective medium modelling and joint inversion of seismic and production data, Journal of Seismic Exploration, 16, 175–97.

Jakobsen, M. (2007c): Effective hydraulic properties of fractured reservoirs and composite porous media, Journal of Seismic Exploration, 16, 199-224.

Jakobsen, M. & Shahraini, A. (2008a): Improved characterization of fractured reservoirs from joint inversion of seismic AVAZ and production data, 70th EAGE meeting, Rome, Italy, Expanded Abstracts, I006.

Jakobsen, M. & Shahraini, A. (2008b): Anisotropic permeability in fractured reservoirs from joint inversion of seismic AVAZ and production data, Proceedings of the 11th European Conference on the Mathematics of Oil recovery, Bergen, Norway, Expanded Abstracts, B02.

Jakobsen, M. & Chapman, M.(2009): Unified theory of global flow and squirt flow in cracked porous media, Geophysics, 74, WA65-WA76.

Kachanov, M. (1980): Continuum model of medium with cracks, Journal of the Engineering Mechanics division, 106, 1039-51.

Kachanov, M. (1992): Elastic properties of cracked solids: Critical review of some basic concepts, Applied Mechanics Reviews, 45, 304–335.

Kachanov, M., Shafiro, B., & Tsukrov, I. (2003): Handbook of elasticity solutions, Kluwer Academic Publishers.

King, M.S. (2002): Elastic wave propagation in and permeability of for rocks with multiple parallel fractures, International Journal of Rock Mechanics and Mining Sciences, 39, 1033-43.

Krebes, E.S. (2004): Seismic forward modelling, CSEG RECORDER, 28-39.

Kseniya, H. (2010): Improved characterization of faulted reservoirs by joint inversion of seismic and production data, Master thesis, University of Bergen, Norway.

Larson, B. (2009): Field and Numerical Studies of Fracture Propagation and Linkage in Limestones: Implications for Permeability, Dissertation for the degree of philosophiae doctor (PhD), University of Bergen, Norway.

Liu, E., Hudson, J.A., & Pointer, T. (2000): Equivalent medium representation of cracked rock, Journal of Geophysical Research, 105, 2981–3000.

Liu, E.R. (2005): Effects of fracture aperture and roughness on hydraulic and mechanical properties of rocks: implication of seismic characterization of fractured reservoirs. Journal of Geophysics and Engineering, 2, 38-47.

Liu, E., Chapman, M., & Tod, S.R. (2007a): Analysis of travel-time and attenuation anisotropy in walkaround and walkaway VSPs from Tiguentourine field, Algeria, Extended abstract, 69th EAGE Conference and Exhibition, London UK, 11-14 June.

Liu, E., Chapman M., Varela, I., Li, X., Queen J.H., & Lynn, H. (2007b): Velocity and attenuation anisotropy: Implication of seismic fracture characterizations, The leading Edge, 26, 1170-74.

Liu, N. & Oliver, D.S. (2003): Evaluation of Monte Carlo methods for assessing uncertainty, SPE Journal, June, 188-95.

Lynn, H.B., Simon, K.M., Bates, C.R., Layman, M., Schneider, R., & Jones, M. (1995): Use of anisotropy in P-wave and S-wave data for fracture characterization in a naturally fractured gas reservoir, The leading edge, 14, 887-93.

Lynn, H.B., Beckham, W.E., Simon, K.M., Bates, C.R., Layman, M., & Jones, M., (1999): P-wave and S-wave azimuthal anisotropy at a naturally fractured gas reservoir, Bluebell-Altamont field, Utah, Geophysics, 64, 1312-28.

MacBeth, C. & Pickup, G. (2002): Estimation of directional permeability in fractured reservoirs - concepts and applications, SEG Expanded Abstract, 21, 97-100.

Maultzsch, S., Chapman, M., Liu, E., & Li, X.Y. (2003): Modelling frequency-dependent seismic anisotropy in fluid-saturated rock with aligned fractures: implication of fracture size estimation from anisotropic measurements, Geophysical Prospecting, 51, 381-92.

Maultzsch, S., Chapman, M., Liu, E., & Li, X.Y. (2007): Modelling and analysis of attenuation anisotropy in multi-azimuth VSP data from the Clair field, Geophysical Prospecting, 55, 627-42.

Mavko, G., Mukerji, T., & Dvorkin, J. (2009): The Rock Physics Handbook, Tools for seismic analysis in porous media, Cambridge University Press, ISBN 978-0-521-86136-6.

Metroplois, N. & Ulam, S. (1949): The Monte Carlo method, Journal of the American Statistical Association, 44, 335-41.

Metropolis, N., Rosenbluth, A.W., Rosenbluth, M.N., Teller, A.H., & Teller, E. (1953): Equations of state calculations by fast computing machines, The Journal of Chemical physics, 21, 1087-92.

Müller, T.M., Gurevich, B., & Lebedev, M. (2010): Seismic wave attenuation and dispersion resulting from wave-induced flow in porous rocks - A review, Geophysics, 75, 75A147-75A164.

Nelson, R.A. (2001): Geologic Analysis of Naturally Fractured Reservoirs, Gulf Professional Publishing, ISBN: 0-88415-317-7.

Nolen-Hoksema, R.C., Wang, Z., Harris, J.M., Langan, R.T. (1995): High-resolution imaging of a West Texan carbonate reservoir: Part 5 – Core analysis, Geophysics, 60, 712-26.

Nishizawa, O. (1982): Seismic velocity anisotropy in a medium containing oriented cracks - Transversely isotropic case, Journal of Physics of the Earth, 30, 331–47.

O'Connell, R.J., & Budiansky, B. (1974): Seismic velocities in dry and saturated cracked solids: Journal of Geophysical Research, 79, 5412–26.

Oda, M. (1985): Permeability tensor for discontinuous rock masses, Geotechnique, 35, 483–95.

Pozdniakov, S. & Tsang C.F. (2004): A self-consistent approach for calculating the effective hydraulic conductivity of a binary, heterogeneous medium, Water Resources Research, 40, W05105, (10.1029/2003WR002617).

Pyrak-Nolte, L.J. & Morris, J.P. (2000): Single fractures under normal stress: the relation between fracture specific stiffness and fluid flow, International Journal of Rock Mechanics and Mining Sciences, 37, 245-62.

Rasolofosaon, P.N.J. & Zinszner, B.E. (2002): Comaprison between permeability anisotropy and elasticity anisotropy of reservoir rocks, Geophysics 67(1), 230-40.

Rogers, S.C., Macbeth, C., Liu, E., & Angerer, E. (2003): Constraining models of fractured reservoirs using seismic anisotropy maps for improved reservoir performance and prediction, 73rd Annual International Meeting, SEG, Expanded Abstracts, 47-50.

Ross, S.M. (1997): Simulation, Second Edition, Orlando, FL: Academic Press.

Rüger, A. (1998): Variation of P-wave reflectivity with offset and azimuth in anisotropic media, Geophysics, 63, 935-47.

Rüger, A. (2002): Reflection coefficients and azimuthal AVO analysis in anisotropic media, Geophysical monograph series, SEG. ISBN 1560801077.

Rykkelid, E. & Fossen, H. (2002): Layer rotation around vertical fault overlap zones: Observations from seismic data, field examples and physical experiments: Marine and Petroleum Geology, 19, 181-92.

Sambridge, M. & Mosegaard, K. (2002): Monte Carlo methods in geophysical inverse problems, Reviews of Geophysics, 40, **3**-1-**3**-29.

Sayers, C.M. (2009): Seismic characterization of reservoirs containing multiple fracture sets, Geophysical Prospecting, 57, 187-92.

Schoenberg, M. (1980): Elastic wave behavior across linear slip interfaces, Journal of the Acoustic Society ofAmerica, 68, 1516–21.

Schoenberg, M. & Protazio, J. (1992): Zeoppritz rationalized and generalized to anisotropy Journal of Seismic Exploration, 1, 125-44.

Schoenberg, M. & Sayers, C.M. (1995): Seismic anisotropy of fractured rock, Geophysics, 60, 204–211.

Sen, M, (2006): Seismic inversion, Society of Petroleum Engineers, U.S.A.

Shahraini, A., Ali, A., & Jakobsen, M. (2010): Seismic history matching in fractured reservoirs using a consistent stiffness-permeability model: Focus on the effects of fracture aperture, Geophysical Prospecting, 59, 492-505.

Sheng, P. (1990): Effective-medium theory of sedimentary rocks, Physical Review B, 41, 4507–11.

Sternlof, K.R., Chapin, J.R., Pollard, D.D., & Durlofsky, L.J. (2004): Permeability effects of deformation bands arrays in sandstone, AAPG Bulletin, 88, 1315–29.

Steve, L., Marrett, R., & Olson, J. (2000): New directions in fracture characterization, The Leading Edge, Geologic Coloumn, July 2000, 704-11.

Tarantola, A. (2005): Inverse Problem Theory and Methods for Model Parameter Estimation, Society for Industrial and Applied Mathematics, (Philadelphia, PA: SIAM).

Tod, S.R. (2001): The effects on seismic waves of interconnected nearly aligned cracks, Geophysical Journal International, 146, 249-263.

Torabi, A. & Fossen, H. (2009): Spatial variation of microstructure and petrophysical properties along deformation bands in reservoir sandstones, AAPG Bulletin, 93, 919–38.

Van Golf-Racht T.D. (1982): Fundamentals of fractured reservoirs engineering, Elsevier, ISBN 0444416250.

Will, R., Archer, R., & Dershowitz, B. (2005): Integration of seismic anisotropy and reservoir-performance data for characterization of naturally fractured reservoirs using discrete fracture network models, SPE meeting, Expanded Abstracts, SPE 84412.

Willis, J.R. (1977): Bounds and self-consistent estimates for the overall properties of anisotropic composites, Journal of the Mechanics and Physics of Solids, 25, 185–202.

Wood, A.W. (1955): A textbook of sound, The Macmillan Co., New York.

Zhang, Y., Sayers, C.M., & Adachi, J.I. (2009): The use of effective medium theories for seismic wave propagation and fluid flow in fractured reservoirs under applied stress, Geophysical Journal international, 177, 205-221.

Zhu, P., Wang, W., Yu, W., & Zhu, G. (2004): Inverting reservoir crack density from P-wave AVOA data, Journal of Geophysics and Engineering, 1, 168-175.

Appendix-A T-matrix approach for effective elastic stiffness tensor

The derivation of the effective stiffness tensor using T-matrix approach is taken from Jakobsen et al., (2003a). The stress tensor $\boldsymbol{\sigma}(\mathbf{x})$ and the strain tensor $\boldsymbol{\varepsilon}(\mathbf{x})$ at point $\mathbf{x}$ of an elastic sample with complex microstructure occupying a large spherical region Ω can be related by linear transformation, under a deformation with infinitesimal strain

$$\boldsymbol{\sigma}(\mathbf{x}) = \mathbf{C}(\mathbf{x})\boldsymbol{\varepsilon}(\mathbf{x}), \tag{A-1}$$

where $\mathbf{C}(\mathbf{x})$ is the local tensor of elastic constants, which reflects the complex microstructure of the sample varying with $\mathbf{x}$ in a random manner, on a scale that is small compared with all other length-scales. For the heterogeneous material as a whole, similar relation in terms of the averaged stress tensor $\langle\boldsymbol{\sigma}(\mathbf{x})\rangle$ and strain tensor $\langle\boldsymbol{\varepsilon}(\mathbf{x})\rangle$ gives

$$\langle\boldsymbol{\sigma}(\mathbf{x})\rangle = \mathbf{C}^{*}\langle\boldsymbol{\varepsilon}(\mathbf{x})\rangle, \tag{A-2}$$

then our problem is to determine the tensor $\mathbf{C}^{*}$ of effective elastic constants using the statistical information about $\mathbf{C}(\mathbf{x})$. The angular brackets $\langle\cdot\rangle$ in Equation (A-2) denote the ensemble average, which can be replaced by the volume average if the material is statistically homogeneous, which means that any sufficiently large sub-regions of Ω is statistically identical with the whole specimen and all ensemble-averaged material quantities, such as $\mathbf{C}^{*}$, are independent of position.

To evaluate the tensor of effective elastic constants from Equation (A-2) an integral equation for the strain tensor field is introduced

$$\boldsymbol{\varepsilon}(\mathbf{x}) = \frac{1}{2}\left\{\nabla\mathbf{u}(\mathbf{x}) + [\nabla\mathbf{u}(\mathbf{x})]^{T}\right\}, \tag{A-3}$$

under a known displacement $\mathbf{u}(\mathbf{x})$ of the surface $\partial\Omega$ of the sample Ω:

$$\mathbf{u}(\mathbf{x}) = \mathbf{U}(\mathbf{x}), \qquad \mathbf{x} \in \partial\Omega. \tag{A-4}$$

Now starting with equilibrium equation

$$\nabla \cdot \boldsymbol{\sigma}(\mathbf{x}) = 0, \tag{A-5}$$

and since the material is homogenous on the macroscopic scale, it can be written as

$$\mathbf{C}(\mathbf{x}) = \mathbf{C}^{(0)} + \delta\mathbf{C}(\mathbf{x}), \tag{A-6}$$

where $\delta\mathbf{C}(\mathbf{x})$ is the fluctuation of $\mathbf{C}(\mathbf{x})$ from a quantity $\mathbf{C}^{(0)}$ which is uniform in space. From equations (A-1), (A-5) and (A-6) it can be written as

$$\nabla \cdot \left[\mathbf{C}^{(0)} \boldsymbol{\varepsilon}(\mathbf{x})\right] = -\nabla \cdot \left[\delta\mathbf{C}(\mathbf{x})\boldsymbol{\varepsilon}(\mathbf{x})\right]. \tag{A-7}$$

An integral equation for the strain field can be derived from the differential equation (Equation (A-7))

$$\boldsymbol{\varepsilon}(\mathbf{x}) = \boldsymbol{\varepsilon}^{(0)} + \int_{\Omega} d\mathbf{x}' \mathbf{G}^{(0)}(\mathbf{x})(\mathbf{x} - \mathbf{x}')\delta\mathbf{C}(\mathbf{x}')\boldsymbol{\varepsilon}(\mathbf{x}'), \tag{A-8}$$

where $\boldsymbol{\varepsilon}^{(0)}$ is the strain tensor due to the boundary displacements in a material with properties given by $\mathbf{C}^{(0)}$. $\mathbf{G}^{(0)}(\mathbf{x})$ is the strain Green's tensor function for a translation-invariant system where the components are given by

$$G_{ijkl}^{(0)}(\mathbf{x}) = -\frac{1}{4}\left[\frac{g_{ik}^{0}(\mathbf{x})}{\partial x_j \partial x_l} + \frac{g_{jk}^{(0)}(\mathbf{x})}{\partial x_i \partial x_l} + \frac{g_{il}^{(0)}(\mathbf{x})}{\partial x_j \partial x_k} + \frac{g_{jl}^{(0)}(\mathbf{x})}{\partial x_i \partial x_k}\right]. \tag{A-9}$$

Here $g_{ik}^{(0)}(\mathbf{x})$ is a component of the displacement Green's tensor function $\mathbf{g}^{(0)}(\mathbf{x})$ which vanishes at the boundary of Ω

$$C_{ijkl}^{(0)} \frac{\partial^2 g_{km}^{(0)}(\mathbf{x})}{\partial x_j x_l} + \delta_{im}\delta(\mathbf{x}) = 0, \qquad \mathbf{g}^{(0)}(\mathbf{x}) = 0 \text{ if } \mathbf{x} \in \partial\Omega. \tag{A-10}$$

Now introducing a fourth-rank tensor field $\mathbf{T}(\mathbf{x})$ which, when contracted with $\boldsymbol{\varepsilon}^{(0)}$ on the right, yields the stress difference $\delta\mathbf{C}(\mathbf{x})\boldsymbol{\varepsilon}(\mathbf{x})$

$$\delta\mathbf{C}(\mathbf{x})\boldsymbol{\varepsilon}(\mathbf{x}) = \mathbf{T}(\mathbf{x})\boldsymbol{\varepsilon}^{(0)}. \qquad (A\text{-}11)$$

$\boldsymbol{\varepsilon}(\mathbf{x})$ is linearly dependent on $\boldsymbol{\varepsilon}^{(0)}$ through the boundary condition (Equation (A-4)), so $\mathbf{T}(\mathbf{x})$ depends only on the material properties and not on $\boldsymbol{\varepsilon}(\mathbf{x})$ or $\boldsymbol{\varepsilon}^{(0)}$. Next step is to find a similar integral equation for $\mathbf{T}(\mathbf{x})$ like in Equation (A-8). Using Equation (A-11) in Equation (A-8), it can be written as

$$\boldsymbol{\varepsilon}(\mathbf{x}) = \boldsymbol{\varepsilon}^{(0)} + \int_{\Omega} d\mathbf{x}' \mathbf{G}^{(0)}(\mathbf{x} - \mathbf{x}')\mathbf{T}(\mathbf{x}')\boldsymbol{\varepsilon}^{(0)}. \qquad (A\text{-}12)$$

By multiplying equation (A-12) with $\delta\mathbf{C}(\mathbf{x})$ from the left and using Equation (A-11) again, it can be obtained

$$\mathbf{T}(\mathbf{x})\boldsymbol{\varepsilon}^{(0)} = \delta\mathbf{C}(\mathbf{x})\boldsymbol{\varepsilon}^{(0)} + \delta\mathbf{C}(\mathbf{x}) \int_{\Omega} d\mathbf{x}' \mathbf{G}^{(0)}(\mathbf{x} - \mathbf{x}')\mathbf{T}(\mathbf{x}')\boldsymbol{\varepsilon}^{(0)}. \qquad (A\text{-}13)$$

The elements T_{ijkl} of $\mathbf{T}$ is chosen to be symmetric in (i,j) and (k,l) and, since $\boldsymbol{\varepsilon}^{(0)}$ may be chosen to be an arbitrary symmetric matrix, it follows that

$$\mathbf{T}(\mathbf{x}) = \delta\mathbf{C}(\mathbf{x}) + \delta\mathbf{C}(\mathbf{x}) \int_{\Omega} d\mathbf{x}' \mathbf{G}^{(0)}(\mathbf{x} - \mathbf{x}')\mathbf{T}(\mathbf{x}'). \qquad (A\text{-}14)$$

The tensor field $\mathbf{T}(\mathbf{x})$ specifies the 'transitions' out of the reference field $\boldsymbol{\varepsilon}^{(0)}$ and gives the complete information about the strain tensor field distribution $\boldsymbol{\varepsilon}(\mathbf{x})$ in the micro-inhomogeneous material, provided that we can solve the integral equation (Equation (A-14)).

For finding the effective elastic constants in terms of $\mathbf{T}$, Equations (A-1) and (A-6) give

$$\langle \boldsymbol{\sigma} \rangle = \mathbf{C}^{(0)}\langle \boldsymbol{\varepsilon} \rangle + \langle \delta\mathbf{C}\boldsymbol{\varepsilon} \rangle. \qquad (A\text{-}15)$$

By combining Equations (A-11) and (A-15) we get

$$\langle \boldsymbol{\sigma} \rangle = \mathbf{C}^{(0)} \langle \boldsymbol{\varepsilon} \rangle + \langle \mathbf{T} \rangle \boldsymbol{\varepsilon}^{(0)}. \tag{A-16}$$

From Equation (A-12) it is clear that

$$\langle \boldsymbol{\varepsilon} \rangle = \boldsymbol{\varepsilon}^{(0)} + \overline{\mathbf{G}} \langle \mathbf{T} \rangle \boldsymbol{\varepsilon}^{(0)}, \tag{A-17}$$

where

$$\overline{\mathbf{G}} = \int_{\Omega} dx' \mathbf{G}^{(0)}(\mathbf{x} - \mathbf{x}'), \qquad \mathbf{x} \in \Omega \tag{A-18}$$

is a constant tensor (Eshelby, 1957). Equation (A-17) gives $\boldsymbol{\varepsilon}^{(0)}$ in terms of $\langle \boldsymbol{\varepsilon} \rangle$

$$\boldsymbol{\varepsilon}^{(0)} = (\mathbf{I} + \overline{\mathbf{G}} \langle \mathbf{T} \rangle)^{-1} \langle \boldsymbol{\varepsilon} \rangle, \tag{A-19}$$

where $\mathbf{I}$ is the identity tensor. Equations (A-2), (A-16) and (A-19), imply that

$$\mathbf{C}^* = \mathbf{C}^{(0)} + \langle \mathbf{T} \rangle (\mathbf{I} + \overline{\mathbf{G}} \langle \mathbf{T} \rangle)^{-1}. \tag{A-20}$$

Equation (A-20) represents a formal exact solution for the case of local elasticity in terms of the T-matrix for the material. Next, a material was considered in which $\mathbf{C}(\mathbf{x})$ is piecewise constant, or specifically a media is considered with inclusions that were either embedded in a homogenous matrix material or else make up a granular aggregate. The population of inclusions is divided into families of inclusions having the same shape/orientation and stiffness tensor $\mathbf{C}^{(r)}$, labeled by $r = 1, 2, ..., R$. Dry cavities may formally be treated as inclusions having vanishing stiffnesses (see Jakobsen et al., 2003a). It was assumed that there were $n^{(r)}$ inclusions of type r, occupying identical regions $\Omega_\alpha^{(r)}$ of the space Ω, centered at random points $\mathbf{x}_\alpha^{(r)}$ $(\alpha = 1, ..., n^{(r)})$. Denote by $\theta^{(r)}(\mathbf{x})$ the characteristic function of the domain $\Omega_\alpha^{(r)}$ (that is, $\theta^{(r)}(\mathbf{x} - \mathbf{x}_\alpha^{(r)}) = 1$, if $\mathbf{x} \in \Omega_\alpha^{(r)}$ and 0 otherwise). It follows that the fluctuation $\delta \mathbf{C}(\mathbf{x})$ may be decomposed as

$$\delta \mathbf{C}(\mathbf{x}) = \sum_{r=1}^{R} \sum_{\alpha=1}^{n^{(r)}} \delta \mathbf{C}_{\alpha}^{(r)}(\mathbf{x}), \tag{A-21}$$

$$\delta \mathbf{C}_{\alpha}^{(r)}(\mathbf{x}) = \delta \mathbf{C}^{(r)} \theta^{(r)}(\mathbf{x} - \mathbf{x}_{\alpha}^{(r)}), \tag{A-22}$$

$$\delta \mathbf{C}^{(r)} = \mathbf{C}^{(r)} - \mathbf{C}^{(0)}. \tag{A-23}$$

A decomposition of the T-matrix for the material, which is analogous with that of $\delta \mathbf{C}(\mathbf{x})$ in Equation (A-21), is given by

$$\mathbf{T}(\mathbf{x}) = \sum_{r=1}^{R} \sum_{\alpha=1}^{n^{(r)}} \mathbf{T}_{\alpha}^{(r)}(\mathbf{x}), \tag{A-24}$$

$$\mathbf{T}_{\alpha}^{(r)}(\mathbf{x}) = \mathbf{T}(\mathbf{x}) \theta^{(r)}(\mathbf{x} - \mathbf{x}_{\alpha}^{(r)}). \tag{A-25}$$

Equations (A-14), (A-21) and (A-24) imply that the $\mathbf{T}_{\alpha}^{(r)}(\mathbf{x})$ must satisfy

$$\mathbf{T}_{\alpha}^{(r)}(\mathbf{x}) = \delta \mathbf{C}_{\alpha}^{(r)}(\mathbf{x}) + \delta \mathbf{C}_{\alpha}^{(r)}(\mathbf{x}) \int_{\Omega} d\mathbf{x}' \mathbf{G}^{(0)}(\mathbf{x} - \mathbf{x}') \sum_{s,\beta} \mathbf{T}_{\beta}^{(s)}(\mathbf{x}'). \tag{A-26}$$

Let $\mathbf{t}_{\alpha}^{(r)}(\mathbf{x})$ denote the solution of the integral equation

$$\mathbf{t}_{\alpha}^{(r)}(\mathbf{x}) = \delta \mathbf{C}_{\alpha}^{(r)}(\mathbf{x}) + \delta \mathbf{C}_{\alpha}^{(r)}(\mathbf{x}) \int_{\Omega} d\mathbf{x}' \mathbf{G}^{(0)}(\mathbf{x} - \mathbf{x}') \mathbf{t}_{\alpha}^{(r)}(\mathbf{x}'), \tag{A-27}$$

then the expression (A-26) for $\mathbf{T}_{\alpha}^{(r)}(\mathbf{x})$ can be written exactly as

$$\mathbf{T}_{\alpha}^{(r)}(\mathbf{x}) = \mathbf{t}_{\alpha}^{(r)}(\mathbf{x}) + \mathbf{t}_{\alpha}^{(r)}(\mathbf{x}) \int_{\Omega} d\mathbf{x}' \mathbf{G}^{(0)}(\mathbf{x} - \mathbf{x}') \sum_{s,\beta} \mathbf{T}_{\beta}^{(s)}(\mathbf{x}')(1 - \delta_{rs} \delta_{\alpha\beta}). \tag{A-28}$$

The solution of the integral equation in the form of $\mathbf{t}_{\alpha}^{(r)}(\mathbf{x})$ infact completely solves the single-body problem. The second term on the right hand side of Equation (A-28) describes the interaction of different bodies or inclusions (Jakobsen et al., 2003a). Successive iterations of Equation (A-28) will lead to the many-body problem. To avoid the complicated calculations of the many-body problem, we restrict ourselves to

the two-body problem based on two-point statistics. A single iteration of Equation (A-28) yields

$$\mathbf{T}_\alpha^{(r)}(\mathbf{x}) \approx \mathbf{t}_\alpha^{(r)}(\mathbf{x}) + \mathbf{t}_\alpha^{(r)}(\mathbf{x}) \int_\Omega d\mathbf{x}' \mathbf{G}^{(0)}(\mathbf{x} - \mathbf{x}') \sum_{s,\beta} \mathbf{t}_\beta^{(s)}(\mathbf{x}')(1 - \delta_{rs}\delta_{\alpha\beta}) . \tag{A-29}$$

Now assuming that the inclusions are ellipsoidal in shape, the T-matrix for a single inclusion can be found. The transition tensor $\mathbf{t}_\alpha^{(r)}(\mathbf{x})$ satisfies (see Equation (A-11))

$$\delta\mathbf{C}_\alpha^{(r)}(\mathbf{x})\boldsymbol{\varepsilon}_\alpha^{(r)}(\mathbf{x}) = \mathbf{t}_\alpha^{(r)}(\mathbf{x})\boldsymbol{\varepsilon}^{(0)} , \tag{A-30}$$

where $\boldsymbol{\varepsilon}_\alpha^{(r)}(\mathbf{x})$ is the strain field for a single inclusion of type r embedded in the homogenous matrix. If $\boldsymbol{\varepsilon}_\alpha^{(r)}(\mathbf{x})$ is constant within the inclusion, then $\mathbf{t}_\alpha^{(r)}(\mathbf{x})$ must also be; and it is zero outside, so it can be written as

$$\mathbf{t}_\alpha^{(r)}(\mathbf{x}) = \mathbf{t}^{(r)}\theta^{(r)}(\mathbf{x} - \mathbf{x}_\alpha^{(r)}), \tag{A-31}$$

where $\mathbf{t}^{(r)}$ is a constant tensor. Inserting this into the integral equation (Equation (A-27)), it can be found

$$\mathbf{t}^{(r)}\theta^{(r)}(\mathbf{x} - \mathbf{x}_\alpha^{(r)}) = \delta\mathbf{C}^{(r)}\theta^{(r)}(\mathbf{x} - \mathbf{x}_\alpha^{(r)}) + \delta\mathbf{C}^{(r)}\theta^{(r)}(\mathbf{x} - \mathbf{x}_\alpha^{(r)}) \int_\Omega d\mathbf{x}' \mathbf{G}^{(0)}(\mathbf{x} - \mathbf{x}')\mathbf{t}^{(r)}\theta^{(r)}(\mathbf{x}' - \mathbf{x}_\alpha^{(r)}) .$$

$$\tag{A-32}$$

Integrating over Ω it can be obtained

$$\mathbf{t}^{(r)} = \delta\mathbf{C}^{(r)} + \delta\mathbf{C}^{(r)}\mathbf{G}^{(r)}\mathbf{t}^{(r)} , \tag{A-33}$$

or

$$\mathbf{t}^{(r)} = (\mathbf{I} - \delta\mathbf{C}^{(r)}\mathbf{G}^{(r)})^{-1}\delta\mathbf{C}^{(r)} , \tag{A-34}$$

where

$$\mathbf{G}^{(r)} = \frac{1}{|\Omega^{(r)}|} \int_{\Omega^{(r)}} d\mathbf{x} \int_{\Omega^{(r)}} d\mathbf{x}' \mathbf{G}^{(0)}(\mathbf{x} - \mathbf{x}') , \tag{A-35}$$

and $\Omega^{(r)}$ is the region of an inclusion of type r centered at the origin. Clearly, $\mathbf{G}^{(r)}$ is a constant tensor, and its components can be evaluated by using the formulae discussed in appendix-B.

From Equations (A-24), (A-29) and (A-31), it can be found

$$\mathbf{T}(\mathbf{x}) \approx \mathbf{T}_1(\mathbf{x}) + \mathbf{T}_2(\mathbf{x}), \tag{A-36}$$

where

$$\mathbf{T}_1(\mathbf{x}) = \sum_r \mathbf{t}^{(r)} \bar{\theta}^{(r)}(\mathbf{x}), \tag{A-37}$$

$$\mathbf{T}_2(\mathbf{x}) = \sum_r \sum_s \mathbf{t}^{(r)} \int_\Omega d\mathbf{x}' \mathbf{G}^{(0)}(\mathbf{x} - \mathbf{x}') \bar{\theta}^{(r)}(\mathbf{x}) \bar{\theta}^{(s)}(\mathbf{x}') \mathbf{t}^{(s)}$$

$$- \sum_{r,\alpha} \mathbf{t}^{(r)} \theta^{(r)}(\mathbf{x} - \mathbf{x}_\alpha^{(r)}) \int_\Omega d\mathbf{x}' \mathbf{G}^{(0)}(\mathbf{x} - \mathbf{x}') \theta^{(r)}(\mathbf{x}' - \mathbf{x}_\alpha^{(r)}) \mathbf{t}^{(r)}, \tag{A-38}$$

and

$$\bar{\theta}^{(r)}(\mathbf{x}) = \sum_\alpha \theta^{(r)}(\mathbf{x} - \mathbf{x}_\alpha^{(r)}), \tag{A-39}$$

is the indicator function of phase r.

In order to evaluate the effective elastic constants from Equation (A-20), or from some equation implied by it, an equivalent $\langle \mathbf{T} \rangle$ is needed to be constructed. From Equation (A-36), it can be obtained

$$\langle \mathbf{T} \rangle \approx \langle \mathbf{T}_1 \rangle + \langle \mathbf{T}_2 \rangle. \tag{A-40}$$

Equation (A-37) yields

$$\langle \mathbf{T}_1 \rangle = \sum_r \mathbf{t}^{(r)} v^{(r)}, \tag{A-41}$$

where

$$v^{(r)} = \left\langle \overline{\theta}^{(r)}(\mathbf{x}) \right\rangle, \tag{A-42}$$

is the relative volume concentration of phase r. From Equation (A-38) it can be obtained

$$\left\langle \mathbf{T}_2 \right\rangle = \sum_r \sum_s \mathbf{t}^{(r)} \int_\Omega d\mathbf{x}' \mathbf{G}^{(0)}(\mathbf{x} - \mathbf{x}') \left\langle \overline{\theta}^{(r)}(\mathbf{x}) \overline{\theta}^{(s)}(\mathbf{x}') \right\rangle \mathbf{t}^{(s)} - \sum_r \mathbf{t}^{(r)} \widetilde{\mathbf{G}}^{(r)} \mathbf{t}^{(r)}, \tag{A-43}$$

where

$$\widetilde{\mathbf{G}}^{(r)} = \sum_\alpha \frac{1}{|\Omega|} \int_\Omega d\mathbf{x} \theta^{(r)}(\mathbf{x} - \mathbf{x}_\alpha^{(r)}) \int_\Omega d\mathbf{x}' \mathbf{G}^{(0)}(\mathbf{x} - \mathbf{x}') \theta^{(r)}(\mathbf{x}' - \mathbf{x}_\alpha^{(r)}), \tag{A-44}$$

and the ensemble average of the second term on the right-hand side of Equation (A-38) is replaced by its volume average. Equations (A-35) and (A-44) imply that

$$\widetilde{\mathbf{G}}^{(r)} = v^{(r)} \mathbf{G}^{(r)}, \tag{A-45}$$

since

$$v^{(r)} = \sum_\alpha \frac{\left| \Omega^{(r)} \right|}{|\Omega|} = n^{(r)} \frac{\left| \Omega^{(r)} \right|}{|\Omega|}. \tag{A-46}$$

The exact expression (A-20) for $\mathbf{C}^*$ can be rewritten exactly as

$$(\delta \mathbf{C}^*)^{-1} = \left\langle \mathbf{T} \right\rangle^{-1} + \overline{\mathbf{G}}, \tag{A-47}$$

where

$$\delta \mathbf{C}^* = \mathbf{C}^* - \mathbf{C}^{(0)}. \tag{A-48}$$

Multiplying Equation (A-47) with $\left\langle \mathbf{T} \right\rangle^{-1}$ from the left and using the standard rule for inversion of tensor inner products, it can be obtained

$$\left\langle \mathbf{T}_1 \right\rangle (\delta \mathbf{C}^*)^{-1} = \left[\left\langle \mathbf{T} \right\rangle \left\langle \mathbf{T}_1 \right\rangle^{-1} \right]^{-1} + \left\langle \mathbf{T}_1 \right\rangle \overline{\mathbf{G}}. \tag{A-49}$$

Combining Equations (A-40) and (A-49) it can be written as

$$\langle \mathbf{T}_1 \rangle (\delta \mathbf{C}^*)^{-1} \approx \left[\mathbf{I} + \langle \mathbf{T}_2 \rangle \langle \mathbf{T}_1 \rangle^{-1} \right]^{-1} + \langle \mathbf{T}_1 \rangle \overline{\mathbf{G}} . \tag{A-50}$$

If we now assume that

$$\left\| \langle \mathbf{T}_2 \rangle \langle \mathbf{T}_1 \rangle^{-1} \right\| < 1 , \tag{A-51}$$

where $\|\cdot\|$ denotes a suitable tensor norm, then it follows from Equation (A-50) that $\delta \mathbf{C}^* \approx \delta \mathbf{C}_T^*$ where

$$\langle \mathbf{T}_1 \rangle (\delta \mathbf{C}_T^*) = \mathbf{I} - \langle \mathbf{T}_2 \rangle \langle \mathbf{T}_1 \rangle^{-1} + \langle \mathbf{T}_1 \rangle \overline{\mathbf{G}}. \tag{A-52}$$

After some tensor algebra, this expression can be rewritten for effective material parameters:

$$\delta \mathbf{C}_T^* = \langle \mathbf{T}_1 \rangle (\mathbf{I} - \langle \mathbf{T}_1 \rangle^{-1} \mathbf{X})^{-1}, \tag{A-53}$$

where

$$\mathbf{X} = \langle \mathbf{T}_2 \rangle - \langle \mathbf{T}_1 \rangle \overline{\mathbf{G}} \langle \mathbf{T}_1 \rangle . \tag{A-54}$$

From Equations (A-18), (A-41), (A-42), (A-43), (A-45) and (A-54), it can be written as

$$\mathbf{X} = \sum_r \sum_s \mathbf{t}^{(r)} \langle \mathbf{A}^{(rs)} \rangle \mathbf{t}^{(s)} - \sum_r \mathbf{t}^{(r)} v^{(r)} \mathbf{G}^{(r)} \mathbf{t}^{(r)}, \tag{A-55}$$

where

$$\langle \mathbf{A}^{(rs)} \rangle = \int_{\Omega} d\mathbf{x}' \mathbf{G}^{(0)}(\mathbf{x} - \mathbf{x}') \left[\langle \overline{\theta}^{(r)}(\mathbf{x}) \overline{\theta}^{(s)}(\mathbf{x}') \rangle - \langle \overline{\theta}^{(r)}(\mathbf{x}) \rangle \langle \overline{\theta}^{(s)}(\mathbf{x}') \rangle \right], \tag{A-56}$$

depends only on $\mathbf{C}^{(0)}$ and the stochastic geometry of the microstructure. $\langle \mathbf{A}^{(rs)} \rangle$ can be written as (Ponte Castaneda and Willis, 1995; Jakobsen et al., 2003a)

$$\left\langle \mathbf{A}^{(rs)} \right\rangle = \delta_{rs} v^{(r)} \mathbf{G}^{(s)} - v^{(r)} v^{(s)} \mathbf{G}_d^{(rs)} , \tag{A-57}$$

where

$$\mathbf{G}_d^{(rs)} = \int_{\Omega_d^{(rs)}} d\mathbf{x}' \mathbf{G}^{(0)}(\mathbf{x} - \mathbf{x}'), \qquad \mathbf{x} \in \Omega_d^{(rs)} \tag{A-58}$$

is a spatially invariant tensor since $\Omega_d^{(rs)}$ represents an ellipsoid having the same symmetry as $p^{(s|r)}(\mathbf{z} - \mathbf{z}')$ which, in turn, represents the probability density for finding an inclusion of type s centered at point $\mathbf{z}'$ given that there is an inclusion of type r centered at point $\mathbf{z}$. Since $p^{(s|r)}(\mathbf{z} - \mathbf{z}') = p^{(r|s)}(\mathbf{z}' - \mathbf{z})$ it follows that $\mathbf{G}_d^{(rs)} = \mathbf{G}_d^{(sr)}$. It was assumed that the inclusions do not overlap because an ellipsoid of type r is surrounded by a 'security' ellipsoid $\Omega_d^{(rs)}$, in the sense that $p^{(s|r)}(\mathbf{z}'') = 0$ if $\mathbf{z}'' \in \Omega_d^{(rs)}$. From Equations (A-55) and (A-58) it can be found

$$\mathbf{X} = -\sum_r \sum_s \mathbf{t}^{(r)} v^{(r)} \mathbf{G}_d^{(rs)} \mathbf{t}^{(s)} v^{(s)} . \tag{A-59}$$

From Equations (A-41), (A-48), (A-53) and (A-59), a new expression for the effective elastic constants is obtained

$$\mathbf{C}^* = \mathbf{C}^{(0)} + \sum_r \mathbf{t}^{(r)} v^{(r)} \left[\mathbf{I} + \left(\sum_s \mathbf{t}^{(s)} v^{(s)} \right)^{-1} \sum_u \sum_v \mathbf{t}^{(u)} v^{(u)} \mathbf{G}_d^{(uv)} \mathbf{t}^{(v)} v^{(v)} \right]^{-1} , \tag{A-60}$$

setting

$$\mathbf{C}_1 = \sum_r v^{(r)} \mathbf{t}^{(r)} , \tag{A-61}$$

$$\mathbf{C}_2 = \sum_r \sum_r v^{(r)} \mathbf{t}^{(r)} \mathbf{G}_d^{(rs)} \mathbf{t}^{(s)} v^{(s)} , \tag{A-62}$$

the effective stiffness tensor can be expressed as

$$\mathbf{C}^* = \mathbf{C}^{(0)} + \mathbf{C}_1 (\mathbf{I} + \mathbf{C}_1^{-1} \mathbf{C}_2)^{-1}. \tag{A-63}$$

It is also important to mention that when the *rth* set of inclusions have a spatial distribution described by an orientation distribution function $O^{(r)}(\theta,\psi,\phi)$, the T-matrix for the individual inclusion, $\mathbf{t}^{(r)}$ in Equations (A-61) and (A-62) have to be replaced by the orientation averaged tensor $\bar{\mathbf{t}}^{(r)}$ given by (Mavko et al., 2009; Jakobsen et al., 2003a, b;)

$$\bar{\mathbf{t}}^{(r)} = \int\limits_0^\pi d\theta \sin\theta \int\limits_0^{2\pi} d\psi \int\limits_0^{2\pi} d\phi O^{(r)}(\theta,\psi,\phi)\mathbf{t}^{(r)}(\theta,\psi,\phi). \tag{A-64}$$

The three Euler angles (θ,ψ,ϕ) define the orientation of the ellipsoid with principal axes $X_1 X_2 X_3$ with respect to the fixed global coordinates $x_1 x_2 x_3$, where θ is the angle between the short axis of the ellipsoid and the x_3-axis (Mavko et al., 2009).The orientation averaging of the T-matrix also involves coordinate transformation of the inclusion stiffness tensor $\mathbf{C}^{(r)}$ from the local coordinate system of the inclusion to the global coordinates using the usual transformation laws for the stiffness tensor (Auld, 1990; Mavko et al., 2009) .

Appendix-B Evaluation of the G Tensor

The tensor $\mathbf{G}^{(r)}$ is given by (Jakobsen and Johansen, 2005)

$$\mathbf{G}^{(r)} = -\mathbf{E}^{(r)}\mathbf{S}^{(0)}, \tag{B-1}$$

where $\mathbf{E}^{(r)}$ is the Eshelby tensor of the ellipsoid. The Eshelby tensor generally is given in terms of first and second elliptical integrals (Jakobsen et al., 2003a; Jakobsen and Johansen, 2005). In the case an isotropic material containing spheroidal inclusions with semi-axes $a_1^{(r)} = a_2^{(r)} = a_r$ and $a_3^{(r)} = b_r$ and whose symmetry axis is aligned in x_3-direction, the elliptical integrals can be evaluated analytically (Jakobsen et al., 2003a). If the matrix material is isotropic then the components of $E_{ijkl}^{(r)}$ are given by (Jakobsen and Johansen, 2005)

$$E_{1111}^{(r)} = E_{2222}^{(r)} = \frac{3}{8(1-v)}\frac{\alpha_r^2}{\alpha_r^2-1} + \frac{1}{4(1-v)}\times\left[1-2v-\frac{9}{4(\alpha_r^2-1)}\right]q,$$

$$E_{3333}^{(r)} = \frac{1}{2(1-v)}\left\{1-2v+\frac{3\alpha_r^2-1}{\alpha_r^2-1} - \left[1-2v+\frac{3\alpha_r^2}{\alpha_r^2-1}\right]q\right\},$$

$$E_{1122}^{(r)} = E_{2211}^{(r)} = \frac{1}{4(1-v)}\left\{\frac{\alpha_r^2}{2(\alpha_r^2-1)} - \left[1-2v+\frac{3}{4(\alpha_r^2-1)}\right]q\right\},$$

$$E_{1133}^{(r)} = E_{2233}^{(r)} = \frac{1}{2(1-v)}\left\{\frac{-\alpha_r^2}{\alpha_r^2-1} + \frac{1}{2}\left[\frac{3\alpha_r^2}{\alpha_r^2-1} - (1-2v)\right]q\right\},$$

$$E_{3311}^{(r)} = \frac{1}{2(1-v)}\left\{2v-1-\frac{1}{\alpha_r^2-1} + \left[1-2v+\frac{3}{2(\alpha_r^2-1)}\right]q\right\},$$

$$E_{1212}^{(r)} = \frac{1}{4(1-v)}\left\{\frac{\alpha_r^2}{2(\alpha_r^2-1)} + \left[1-2v-\frac{3}{4(\alpha_r^2-1)}\right]q\right\},$$

$$E_{1313}^{(r)} = E_{2323}^{(r)} = \frac{1}{4(1-v)} \left\{ 1 - 2v - \frac{\alpha_r^2 + 1}{\alpha_r^2 - 1} - \frac{1}{2} \left[1 - 2v - \frac{3(\alpha_r^2 + 1)}{\alpha_r^2 - 1} \right] q \right\},$$ (B-2)

where v is the Poisson ratio of the matrix, $\alpha_r = b_r / a_r$ is the aspect ratio of the rth spheroid, and q is given by

$$q = \frac{\alpha_r}{(1 - \alpha_r^2)^{3/2}} \left[\cos^{-1} \alpha_r - \alpha_r (1 - \alpha_r^2)^{1/2} \right]$$ (B-3)

when $\alpha_r \leq 1$.

From these results it can be written for spheres $(\alpha_r = 1, q = 2/3)$,

$$E_{ijkl}^{(r)} = \frac{5v - 1}{15(1 - v)} \delta_{ij} \delta_{kl} + \frac{4 - 5v}{15(1 - v)} (\delta_{ik} \delta_{jl} + \delta_{il} \delta_{jk}).$$ (B-4)

If r refers to a typical flat compliant Hudson-crack (characterized by $\alpha_r \to 0, q \to 0$), then only non-vanishing components are

$$E_{3333}^{(r)} = 1,$$
$$E_{3311}^{(r)} = S_{3322}^{(r)} = \frac{v}{v - 1},$$ (B-5)
$$E_{1313}^{(r)} = S_{2323}^{(r)} = \frac{1}{2}.$$

The above expressions for the $\mathbf{G}^{(r)}$ tensor can also be used to evaluate the $\mathbf{G}_d^{(rs)}$ tensor.

Appendix-C Equations for a single communicating cavity

The derivation is taken from Jakobsen and Hudson (2003), Jakobsen et al., (2003b) and Jakobsen and Chapman (2009). The t-matrix for a single inclusion of type r is given by (Jakobsen et al., 2003a)

$$\mathbf{t}^{(r)} = (\mathbf{C}^{(r)} - \mathbf{C}^{(0)})\left[\mathbf{I}_4 - \mathbf{G}^{(r)}(\mathbf{C}^{(r)} - \mathbf{C}^{(0)})\right]^{-1}, \tag{C-1}$$

where $\mathbf{I}_4$ is the identity tensor for the fourth-rank tensors. The t-matrix in Equation (C-1) can be expressed with a K-matrix which relates the strain, $\boldsymbol{\varepsilon}^{(r)}$, within an inclusion to the imposed stress at infinity $\boldsymbol{\sigma}^{(0)}$

$$\boldsymbol{\varepsilon}^{(r)} = \mathbf{K}^{(r)}\boldsymbol{\sigma}^{(0)}. \tag{C-2}$$

The $\mathbf{K}$-tensor can be expressed as (Jakobsen et al., 2003b)

$$\mathbf{K}^{(r)} = \left[\mathbf{I}_4 - \mathbf{G}^{(r)}(\mathbf{C}^{(r)} - \mathbf{C}^{(0)})\right]^{-1}\mathbf{S}^{(0)}, \tag{C-3}$$

such that the t-matrix is

$$\mathbf{t}^{(r)} = (\mathbf{C}^{(r)} - \mathbf{C}^{(0)})\mathbf{K}^{(r)}\mathbf{S}^{(0)}. \tag{C-4}$$

The Equation (C-4) means that we can find the t-matrix of a communicating cavity provided that we know the corresponding K-matrix. By linear superposition, the strain inside a fully saturated cavity of type r under fluid pressure $p_f^{(r)}$ and imposed stress $\boldsymbol{\sigma}^{(0)}$ at infinity, is given by the strain within the corresponding dry cavity under the imposed stress $(\boldsymbol{\sigma}^{(0)} + \mathbf{I}_2 p_f^{(r)})$ minus the strain within a similarly shaped and oriented cavity with hydrostatic stress $\mathbf{I}_2 p_f^{(r)}$ applied both at infinity and inside the cavity, where $\mathbf{I}_2$ is the second-rank identity tensor. By using this argument in conjunction with Equations (C-2) and (C-3), it can be written as

$$\mathbf{K}^{(r)}\boldsymbol{\sigma}^{(0)} = \mathbf{K}_d^{(r)}(\boldsymbol{\sigma}^{(0)} + \mathbf{I}_2 p_f^{(r)}) - \mathbf{S}^{(0)}\mathbf{I}_2 p_f^{(r)},$$

(C-5)

where

$$\mathbf{K}_d^{(r)} = (\mathbf{I}_4 + \mathbf{G}^{(n)}\mathbf{C}^{(0)})^{-1}\mathbf{S}^{(0)}, \tag{C-6}$$

is the K-matrix of a dry cavity of type r.

The linearity of the problem suggest that there exists a second-rank tensor $\boldsymbol{\psi}^{(r)}$, which relates the fluid pressure to the applied stress given by

$$p_f^{(r)} = \boldsymbol{\psi}^{(r)}\boldsymbol{\sigma}^{(0)}. \tag{C-7}$$

From Equations (C-5) and (C-7) and using the fact that $\boldsymbol{\sigma}^{(0)}$ is arbitrary, it can be found

$$\mathbf{K}^{(r)} = \mathbf{K}_d^{(r)} + (\mathbf{K}_d^{(r)} - \mathbf{S}^{(0)})(\mathbf{I}_2 \otimes \boldsymbol{\psi}^{(r)}), \tag{C-8}$$

where the symbol $\otimes$ denotes the dyadic tensor product. Inserting Equation (C-8) in to Equation (C-4), an expression for t-matrix can be obtained for a single cavity of type r fully saturated with a homogenous fluid given by

$$\mathbf{t}^{(r)} = \mathbf{t}_d^{(r)} + \mathbf{t}_d^{(r)}\mathbf{S}^{(0)}(\mathbf{I}_2 \otimes \boldsymbol{\psi}^{(r)})\mathbf{C}^{(0)}. \tag{C-9}$$

Now the problem is reduced to the evaluation of the fluid pressure polarization tensor $\boldsymbol{\psi}^{(r)}$. To evaluate the fluid-pressure-polarization tensor $\boldsymbol{\psi}^{(r)}$ in the case of a communicating cavity, we ensure that total fluid mass concentration m_f in an arbitrary volume is conserved. The wave-induced fluid flow at the scale of wavelength is given by Darcy' law (Jakobsen et al., 2003b; Jakobsen and Chapman, 2009)

$$\frac{\partial m_f}{\partial t} = \nabla \cdot \left(\frac{\rho_f}{\eta_f} \boldsymbol{\Gamma} \cdot \nabla p_f \right), \tag{C-10}$$

where ρ_f is the fluid mass density, η_f is the fluid viscosity and Γ is the effective permeability tensor. The pressure and density of the fluid inside the r'th cavity set are related by (Jakobsen et al., 2003b; Jakobsen and Chapman, 2009)

$$\frac{\rho_0}{\rho_f^{(r)}} = 1 - \frac{p_f^{(r)}}{\kappa_f},$$
(C-11)

where ρ_0 is the density of the unstressed fluid and κ_f is the fluid bulk modulus. The fluid pressure of the r'th cavity set will change because of both fluid flow out and porosity change, if a quasi-static stress field is imposed on the arbitrary volume. The first order expression for changes in porosity can be obtained by using the equations (C-2) and (C-6) and is given by (Jakobsen et al., 2003b; Jakobsen and Chapman, 2009)

$$\frac{\widetilde{\varphi}^{(r)} - \varphi^{(r)}}{\varphi^{(r)}} = \mathbf{I}_2 \mathbf{K}_d^{(r)} (\boldsymbol{\sigma}^{(0)} + \mathbf{I}_2 p_f^{(r)}) - \mathbf{I}_2 \mathbf{S}^{(0)} \mathbf{I}_2 p_f^{(r)},$$
(C-12)

where $\widetilde{\varphi}^{(r)}$ is the stressed porosity while $\varphi^{(r)}$ is the unstressed porosity of the r'th cavity set, respectively. The expression for $\mathbf{K}_d^{(r)}$ is given in Equation (C-6).

The expression controlling the fluid-mass flow out of the r'th cavity set in Jakobsen et al., (2003b) has an error related to the conservation of fluid mass, which was corrected by Jakobsen and Chapman (2009). The fluid-mass flow out of the r'th cavity set is given by (Jakobsen and Chapman, 2009)

$$\frac{\partial m_f^{(r)}}{\partial t} - \frac{\varphi^{(r)}}{\varphi} \frac{\partial m_f}{\partial t} = -\frac{\rho_0 \varphi_0^{(r)}}{\kappa_f \tau} (p_f^{(r)} - p_f), \qquad r = 1, ..., N,$$
(C-13)

where τ is the relaxation time constant.

Using Equation (C-7) and working toward first order in Equations (C-11) and (C-12) with the assumption that the propagating-plane harmonic wave has angular frequency ω and the wave vector $\mathbf{k}$, it can written as (Jakobsen and Chapman, 2009)

$$\boldsymbol{\psi}^{(r)} = \frac{(1-\Delta)\boldsymbol{\psi} - i\omega\tau\kappa_f \mathbf{I}_2 \mathbf{K}_d^{(r)}}{1 + i\omega\gamma^{(r)}\tau}, \tag{C-14}$$

and

$$\gamma^{(r)} = 1 + \kappa_f \mathbf{I}_2 (\mathbf{K}_d^{(r)} - \mathbf{S}^{(0)})\mathbf{I}_2, \tag{C-15}$$

where

$$\Delta = \frac{\Gamma_{ij}k_i k_j \kappa_f}{\varphi\eta_f}\tau \tag{C-16}$$

is a new term related to the coupling of the processes of wave induced fluid flow. To find the $\boldsymbol{\psi}$ tensor in Equation (C-14), an expression for m_f using Equations (C-11) and (C-12) is obtained and then inserted into the Equation (C-10) to get

$$\boldsymbol{\psi} = -\boldsymbol{\Theta}\sum_{r=1}^{N} \frac{\varphi^{(r)}\mathbf{I}_2 \mathbf{K}_d^{(r)}}{1 + i\omega\gamma^{(r)}\tau}, \tag{C-17}$$

where

$$\boldsymbol{\Theta} = \kappa_f \left[\sum_{r=1}^{N} \frac{\varphi^{(r)}\gamma^{(r)}}{1 + i\omega\gamma^{(r)}\tau}(1-\Delta) - \frac{i\kappa_f \Gamma_{ij}k_i k_j}{\eta_f \omega} \right]^{-1}. \tag{C-18}$$

From Equations (C-14), (C-17) and (C-18), it can be obtained

$$\boldsymbol{\psi}^{(r)} = \frac{-\widetilde{\boldsymbol{\Theta}}\sum_{r=1}^{N} \frac{\varphi^{(r)}\mathbf{I}_2 \mathbf{K}_d^{(r)}}{1 + i\omega\gamma^{(r)}\tau} - i\omega\tau\kappa_f \mathbf{I}_2 \mathbf{K}_d^{(r)}}{1 + i\omega\gamma^{(r)}\tau}, \tag{C-19}$$

where

$$\widetilde{\boldsymbol{\Theta}} = \kappa_f \left[\sum_{r=1}^{N} \frac{\varphi^{(r)}\gamma^{(r)}}{1 + i\omega\gamma^{(r)}\tau} - \frac{iK_{ij}k_i k_j \kappa_f}{\eta_f \omega(1-\Delta)} \right]^{-1}. \tag{C-20}$$

Appendix D- T-matrix approach for effective permeability tensor

The derivation of the effective permeability tensor using T-matrix approach is taken from Jakobsen (2007c). A permeable specimen with complex meso-structure occupying a large spherical region Ω is assumed. During steady-state flow of a single-phase fluid, the fluid filtration velocity $\mathbf{Q(x)}$ and the pressure gradient $\mathbf{J(x)}$ are related by the Darcy law

$$\mathbf{Q(x)} = \mathbf{K(x)J(x)}, \tag{D-1}$$

where $\mathbf{K(x)}$ is a second-rank tensor of the permeability constants. For a heterogeneous porous medium Equation (D-1) can be written in terms of the averaged fluid filtration velocity $\langle \mathbf{Q(x)} \rangle$ and $\langle \mathbf{J(x)} \rangle$ given by

$$\langle \mathbf{Q(x)} \rangle = \mathbf{K}^* \langle \mathbf{J(x)} \rangle, \tag{D-2}$$

where the $\langle \cdot \rangle$ denote the ensemble average of the which may be related to the volume average if the material is statistically homogeneous. The remaining problem is to determine the effective permeability tensor $\mathbf{K}^*$ using the statistical information we have about $\mathbf{K(x)}$. To evaluate the effective permeability constants in Equation (D-2) an integral equation for pressure gradient field is used

$$\mathbf{J(x)} = \nabla p(\mathbf{x}), \tag{D-3}$$

where $p(\mathbf{x})$ is the known fluid pressure on the surface $\partial\Omega$ of the specimen Ω. The conservation of the fluid mass takes the from for the steady-state flow

$$\nabla \cdot \mathbf{Q(x)} = 0. \tag{D-4}$$

As the medium is homogenous on macroscopic scale, it can be written as

$$\mathbf{K(x)} = \mathbf{K}^{(0)} + \delta\mathbf{K(x)}, \tag{D-5}$$

where $\delta\mathbf{K}(\mathbf{x})$ is the fluctuation of $\mathbf{K}(\mathbf{x})$ from a quantity $\mathbf{K}^{(0)}$ which is uniform in space. Now from Equations (D-1), (D-4) and (D-5), it can be obtained

$$\nabla \cdot \left[\mathbf{K}^{(0)}\mathbf{J}(\mathbf{x})\right] = -\nabla \cdot \left[\delta\mathbf{K}(\mathbf{x})\mathbf{J}(\mathbf{x})\right], \qquad\qquad \text{(D-6)}$$

where the term on the right-hand side can be regarded as an applied source term. An integral equation for pressure gradient can be derived from Equation (D-6)

$$\mathbf{J}(\mathbf{x}) = \mathbf{J}^{(0)} + \int_{\Omega} d\mathbf{x}'\mathbf{G}^{(0)}(\mathbf{x} - \mathbf{x}')\delta\mathbf{K}(\mathbf{x}')\mathbf{J}(\mathbf{x}'), \qquad\qquad \text{(D-7)}$$

where $\mathbf{J}^{(0)}$ is the pressure gradient due to the applied boundary conditions on a material with properties given by $\mathbf{K}^{(0)}$. The components of the dipolar tensor $\mathbf{G}^{(0)}(\mathbf{x} - \mathbf{x}')$ are given by

$$G_{ij}^{(0)}(\mathbf{x}) = \partial^2 g^{(0)}(\mathbf{x})/\partial x_i x_j, \qquad\qquad \text{(D-8)}$$

where the scalar Green's function $g^{(0)}(\mathbf{x})$ is the solution to the flow equation in a homogenous medium with a unit source given by

$$K_{ij}^{(0)}\left[g^{(0)}(\mathbf{x})/\partial x_i x_j\right] = -\delta(\mathbf{x}). \qquad\qquad \text{(D-9)}$$

Following Jakobsen et al., (2003a), a second-rank tensor field $\mathbf{T}(\mathbf{x})$ is introduced which, when contracted with $\mathbf{J}^{(0)}$ on the right, yields the velocity difference $\delta\mathbf{K}(\mathbf{x})\mathbf{J}(\mathbf{x})$

$$\delta\mathbf{K}(\mathbf{x})\mathbf{J}(\mathbf{x}) = \mathbf{T}(\mathbf{x})\mathbf{J}^{(0)}. \qquad\qquad \text{(D-10)}$$

Since $\mathbf{J}(\mathbf{x})$ is linearly dependent on $\mathbf{J}^{(0)}$ through the boundary conditions and $\mathbf{T}(\mathbf{x})$ depends only on the material properties and not on $\mathbf{J}(\mathbf{x})$ or $\mathbf{J}^{(0)}$, then by using Equation (D-10) in (D-7) we get an integral equation similar to Equation (D-7)

$$\mathbf{J}(\mathbf{x}) = \mathbf{J}^{(0)} + \int_{\Omega} d\mathbf{x}'\mathbf{G}^{(0)}(\mathbf{x} - \mathbf{x}')\mathbf{T}(\mathbf{x}')\mathbf{J}^{(0)}. \qquad\qquad \text{(D-11)}$$

Now multiplying Equation (D-11) with $\delta\mathbf{K}(\mathbf{x})$ from the left and using Equation (D-10), it can be written as

$$\mathbf{T}(\mathbf{x})\mathbf{J}^{(0)} = \delta\mathbf{K}(\mathbf{x})\mathbf{J}^{(0)} + \delta\mathbf{K}(\mathbf{x})\int_{\Omega}\mathrm{d}\mathbf{x}'\mathbf{G}^{(0)}(\mathbf{x}-\mathbf{x}')\mathbf{T}(\mathbf{x}')\mathbf{J}^{(0)}. \tag{D-12}$$

Choosing the elements of $\mathbf{T}$ to be symmetric in (i,j) and $\mathbf{J}^{(0)}$ as an arbitrary tensor, it follows

$$\mathbf{T}(\mathbf{x}) = \delta\mathbf{K}(\mathbf{x}) + \delta\mathbf{K}(\mathbf{x})\int_{\Omega}\mathrm{d}\mathbf{x}'\mathbf{G}^{(0)}(\mathbf{x}-\mathbf{x}')\mathbf{T}(\mathbf{x}'). \tag{D-13}$$

Next step is to evaluate the effective permeability constants in terms of ensemble average of $\mathbf{T}$. Using Equations (D-1) to (D-5) and combining the resultant expression with Equation (D-10), it can be obtained

$$\langle\mathbf{Q}\rangle = \mathbf{K}^{(0)}\langle\mathbf{J}\rangle + \langle\mathbf{T}\rangle\mathbf{J}^{(0)}. \tag{D-14}$$

From Equation (D-11) it can be written as

$$\langle\mathbf{J}\rangle = \mathbf{J}^{(0)} + \overline{\mathbf{G}}\langle\mathbf{T}\rangle\mathbf{J}^{(0)}, \tag{D-15}$$

where

$$\overline{\mathbf{G}} = \int_{\Omega}\mathrm{d}\mathbf{x}'\mathbf{G}^{(0)}(\mathbf{x}-\mathbf{x}'), \qquad \mathbf{x}\in\Omega, \tag{D-16}$$

is a constant tensor. Equation (D-15) gives $\mathbf{J}^{(0)}$ in terms of $\langle\mathbf{J}\rangle$:

$$\mathbf{J}^{(0)} = (\mathbf{I}+\overline{\mathbf{G}}\langle\mathbf{T}\rangle)^{-1}\langle\mathbf{J}\rangle, \tag{D-17}$$

where $\mathbf{I}$ is the identity tensor. Equations (D-2), (D-14) and (D-17) imply that

$$\mathbf{K}^{*} = \mathbf{K}^{(0)} + \langle\mathbf{T}\rangle(\mathbf{I}+\overline{\mathbf{G}}\langle\mathbf{T}\rangle)^{-1}. \tag{D-18}$$

Equation (D-18) gives a formal exact solution for the tensor of effective permeability constants of a random medium in terms of ensemble average of the T-matrix of the

medium. The ensemble average of the T-matrix still remains to be determined. The all above equations are valid for the tensor of permeability constants $\mathbf{K}(\mathbf{x})$ arbitrarily varying in space. Now considering a media in which $\mathbf{K}(\mathbf{x})$ is piecewise constant and inclusions are either embedded in the homogeneous matrix material or else make up a composite porous medium. The population of inclusions is divided into families of inclusions having the same shape/orientation and permeability tensor $\mathbf{K}^{(r)}$, labeled by $r = 1, 2, ..., N$. It was also assumed that there are $n^{(r)}$ inclusions of type r, occupying identical regions $\Omega_\alpha^{(r)}$ of the space Ω, centered at random points $\mathbf{x}_\alpha^{(r)}$ $(\alpha = 1, ..., n^{(r)})$. The characteristic function of the domain $\Omega_\alpha^{(r)}$ is denoted by $\theta_\alpha^{(r)}$ and as the medium is piecewise constant we can write it as ($\theta^{(r)}(\mathbf{x} - \mathbf{x}_\alpha^{(r)}) = 1$, if $\mathbf{x} \in \Omega_\alpha^{(r)}$ and 0 otherwise). The fluctuation of $\mathbf{K}(\mathbf{x})$ can be decomposed as

$$\delta\mathbf{K}(\mathbf{x}) = \sum_{r=1}^{N} \sum_{\alpha=1}^{n^{(r)}} \delta\mathbf{K}_\alpha^{(r)}(\mathbf{x}), \tag{D-19}$$

$$\delta\mathbf{K}_\alpha^{(r)}(\mathbf{x}) = \delta\mathbf{K}^{(r)}\theta^{(r)}(\mathbf{x} - \mathbf{x}_\alpha^{(r)}), \tag{D-20}$$

$$\delta\mathbf{K}^{(r)} = \mathbf{K}^{(r)} - \mathbf{K}^{(0)}. \tag{D-21}$$

Similarly, T-matrix of the medium can be decomposed given by

$$\mathbf{T}(\mathbf{x}) = \sum_{r=1}^{N} \sum_{\alpha=1}^{n^{(r)}} \mathbf{T}_\alpha^{(r)}(\mathbf{x}), \tag{D-22}$$

$$\mathbf{T}_\alpha^{(r)}(\mathbf{x}) = \mathbf{T}(\mathbf{x})\theta^{(r)}(\mathbf{x} - \mathbf{x}_\alpha^{(r)}). \tag{D-23}$$

Equations (D-13), (D-19) and (D-22) imply that $\mathbf{T}_\alpha^{(r)}(\mathbf{x})$ must satisfy

$$\mathbf{T}_\alpha^{(r)}(\mathbf{x}) = \delta\mathbf{K}_\alpha^{(r)}(\mathbf{x}) + \delta\mathbf{K}_\alpha^{(r)}(\mathbf{x}) \int_\Omega d\mathbf{x}' \mathbf{G}^{(0)}(\mathbf{x} - \mathbf{x}') \sum_{s,\beta} \mathbf{T}_\beta^{(s)}(\mathbf{x}'). \tag{D-24}$$

From the work of Jakobsen et al., (2003a), Equation (D-24) can be written exactly as

$$\mathbf{T}_\alpha^{(r)}(\mathbf{x}) = \mathbf{t}_\alpha^{(r)}(\mathbf{x}) + \mathbf{t}_\alpha^{(r)}(\mathbf{x}) \int_\Omega d\mathbf{x}' \mathbf{G}^{(0)}(\mathbf{x} - \mathbf{x}') \sum_{s,\beta} \mathbf{T}_\beta^{(s)}(\mathbf{x}')(1 - \delta_{rs}\delta_{\alpha\beta}) , \qquad \text{(D-25)}$$

where $\mathbf{t}_\alpha^{(r)}(\mathbf{x})$ denote the solution of the integral equation and gives us the fluid pressure inside the inclusion (r, α) given by

$$\mathbf{t}_\alpha^{(r)}(\mathbf{x}) = \delta\mathbf{K}_\alpha^{(r)}(\mathbf{x}) + \delta\mathbf{K}_\alpha^{(r)}(\mathbf{x}) \int_\Omega d\mathbf{x}' \mathbf{G}^{(0)}(\mathbf{x} - \mathbf{x}')\mathbf{t}_\alpha^{(r)}(\mathbf{x}') . \qquad \text{(D-26)}$$

Infact $\mathbf{t}_\alpha^{(r)}(\mathbf{x})$ completely solves the single-body problem. The second term on the right hand side of Equation (D-25) describes the interaction of different bodies or inclusions (Jakobsen, 2007). Successive iterations of Equation (D-25) will lead to the many-body problem. To avoid the complicated calculations of the many-body problem, we restrict ourselves to the two-body problem based on two-point statistics. A single iteration of Equation (D-25) yields

$$\mathbf{T}_\alpha^{(r)}(\mathbf{x}) = \mathbf{t}_\alpha^{(r)}(\mathbf{x}) + \mathbf{t}_\alpha^{(r)}(\mathbf{x}) \int_\Omega d\mathbf{x}' \mathbf{G}^{(0)}(\mathbf{x} - \mathbf{x}') \sum_{s,\beta} \mathbf{t}_\beta^{(s)}(\mathbf{x}')(1 - \delta_{rs}\delta_{\alpha\beta}) . \qquad \text{(D-27)}$$

Now, in Equation (D-27) the first term on the right-hand side is related to the single inclusion transition tensor, while the second term on the right-hand side is directly related to interactions between two inclusions, respectively. To evaluate the single transition tensor $\mathbf{t}_\alpha^{(r)}(\mathbf{x})$, the shape of the inclusion is taken to be ellipsoidal and $\mathbf{K}^{(0)}$ corresponds to the properties of the matrix. The transition tensor $\mathbf{t}_\alpha^{(r)}(\mathbf{x})$ satisfies

$$\delta\mathbf{K}_\alpha^{(r)}(\mathbf{x})\mathbf{J}_\alpha^{(r)}(\mathbf{x}) = \mathbf{t}_\alpha^{(r)}(\mathbf{x})\mathbf{J}^{(0)} , \qquad \text{(D-28)}$$

where $\mathbf{J}_\alpha^{(r)}(\mathbf{x})$ is the pressure gradient field for a single inclusion of type r embedded in the homogenous matrix. The $\mathbf{J}_\alpha^{(r)}(\mathbf{x})$ can be written as

$$\mathbf{J}_\alpha^{(r)}(\mathbf{x}) = \mathbf{J}^{(r)}\theta^{(r)}(\mathbf{x} - \mathbf{x}_\alpha^{(r)}) , \qquad \text{(D-29)}$$

where $\mathbf{J}^{(r)}$ is a constant tensor and then $\mathbf{t}_\alpha^{(r)}(\mathbf{x})$ can be written as

$$\mathbf{t}_\alpha^{(r)}(\mathbf{x}) = \mathbf{t}^{(r)}\theta^{(r)}(\mathbf{x} - \mathbf{x}_\alpha^{(r)}) , \qquad \text{(D-30)}$$

where $\mathbf{t}^{(r)}$ is a constant tensor. Using Equation (D-29) in (D-26), it can be obtained

$$\mathbf{t}^{(r)}\theta^{(r)}(\mathbf{x}-\mathbf{x}_\alpha^{(r)}) = \delta\mathbf{K}^{(r)}\theta^{(r)}(\mathbf{x}-\mathbf{x}_\alpha^{(r)}) + \delta\mathbf{K}^{(r)}\theta^{(r)}(\mathbf{x}-\mathbf{x}_\alpha^{(r)})\int_\Omega d\mathbf{x}'\mathbf{G}^{(0)}(\mathbf{x}-\mathbf{x}')\mathbf{t}^{(r)}\theta^{(r)}(\mathbf{x}'-\mathbf{x}_\alpha^{(r)}).$$

(D-31)

Now integrating over Ω, it can be obtained

$$\mathbf{t}^{(r)} = \delta\mathbf{K}^{(r)} + \delta\mathbf{K}^{(r)}\mathbf{G}^{(r)}\mathbf{t}^{(r)},$$

(D-32)

or

$$\mathbf{t}^{(r)} = (\mathbf{I} - \delta\mathbf{K}^{(r)}\mathbf{G}^{(r)})^{-1}\delta\mathbf{K}^{(r)},$$

(D-33)

where

$$\mathbf{G}^{(r)} = \left(1/\left|\Omega^{(r)}\right|\right)\int_{\Omega^{(r)}} d\mathbf{x}\int_{\Omega^{(r)}} d\mathbf{x}'\mathbf{G}^{(0)}(\mathbf{x}-\mathbf{x}'),$$

(D-34)

and $\Omega^{(r)}$ is the region of an inclusion of type r centered at the origin. $\mathbf{G}^{(r)}$ is a constant tensor, and it's components are given by

$$\mathbf{G}_{ii}^{(r)} = -n_i^{(r)}/\mathbf{K}_{ii}^{(0)}, \qquad \text{no sum,}$$

(D-35)

where $n_i^{(r)}$, $i=1,2,3$ are the depolarization coefficients which depend on the shape of the spheroid, given by (Jakobsen, 2007c)

$$n_1^{(r)} = n_2^{(r)} = (1-n_3^{(r)})/2,$$

(D-36)

$$n_3^{(r)} = \left[(1+1_r^2)/1_r^3\right]\left(1_r - \tan^{-1}1_r\right),$$

(D-37)

$$1 = \sqrt{\left\{(\alpha^{(r)})^2(\mathbf{K}_{33}^{(0)}/\mathbf{K}_{11}^{(0)})-1\right\}},$$

(D-38)

and $\alpha^{(r)}$ is the corresponding aspect ratio.

Equations (D-22), (D-27) and (D-30) give

$$\mathbf{T}(\mathbf{x}) = \mathbf{T}_1(\mathbf{x}) + \mathbf{T}_2(\mathbf{x}), \tag{D-39}$$

where

$$\mathbf{T}_1(\mathbf{x}) = \sum_r \mathbf{t}^{(r)} \overline{\theta}^{(r)}(\mathbf{x}), \tag{D-40}$$

$$\mathbf{T}_2(\mathbf{x}) = \sum_r \sum_s \mathbf{t}^{(r)} \int_\Omega d\mathbf{x}' \mathbf{G}^{(0)}(\mathbf{x} - \mathbf{x}') \overline{\theta}^{(r)}(\mathbf{x}) \overline{\theta}^{(s)}(\mathbf{x}') \mathbf{t}^{(s)}$$

$$- \sum_{r,\alpha} \mathbf{t}^{(r)} \theta^{(r)}(\mathbf{x} - \mathbf{x}_\alpha^{(r)}) \int_\Omega d\mathbf{x}' \mathbf{G}^{(0)}(\mathbf{x} - \mathbf{x}') \theta^{(r)}(\mathbf{x}' - \mathbf{x}_\alpha^{(r)}) \mathbf{t}^{(r)}, \tag{D-41}$$

and

$$\overline{\theta}^{(r)}(\mathbf{x}) = \sum_\alpha \theta^{(r)}(\mathbf{x} - \mathbf{x}_\alpha^{(r)}), \tag{D-42}$$

is the indicator for phase r.

An equivalent $\langle \mathbf{T} \rangle$ is needed to be constructed to evaluate the effective permeability constants from Equation (D-2). Equation (D-39) can be written as

$$\langle \mathbf{T} \rangle = \langle \mathbf{T}_1 \rangle + \langle \mathbf{T}_2 \rangle. \tag{D-43}$$

Equation (D-40) yields

$$\langle \mathbf{T}_1 \rangle = \sum_r \mathbf{t}^{(r)} v^{(r)}, \tag{D-44}$$

where

$$v^{(r)} = \left\langle \overline{\theta}^{(r)}(\mathbf{x}) \right\rangle, \tag{D-45}$$

is the relative volume concentration of the phase r.

In Equation (D-41), replacing the ensemble average of the second term on the right hand side by its volume average, it can be written as

$$\langle \mathbf{T}_2 \rangle = \sum_r \sum_s \mathbf{t}^{(r)} \int_\Omega d\mathbf{x}' \mathbf{G}^{(0)}(\mathbf{x}-\mathbf{x}') \langle \overline{\theta}^{(r)}(\mathbf{x}) \overline{\theta}^{(s)}(\mathbf{x}') \rangle \mathbf{t}^{(s)} - \sum_r \mathbf{t}^{(r)} \widetilde{\mathbf{G}}^{(r)} \mathbf{t}^{(r)} ,$$

(D-46)

where

$$\widetilde{\mathbf{G}}^{(r)} = \sum_\alpha \left(1/|\Omega| \right) \int_\Omega d\mathbf{x} \theta^{(r)}(\mathbf{x}-\mathbf{x}_\alpha^{(r)}) \int_\Omega d\mathbf{x}' \mathbf{G}^{(0)}(\mathbf{x}-\mathbf{x}') \theta^{(r)}(\mathbf{x}'-\mathbf{x}_\alpha^{(r)}) .$$

(D-47)

Equations (D-34) and (D-47) imply that

$$\widetilde{\mathbf{G}}^{(r)} = v^{(r)} \mathbf{G}^{(r)} ,$$

(D-48)

since

$$v^{(r)} = \sum_\alpha \frac{|\Omega^{(r)}|}{|\Omega|} = n^{(r)} \frac{|\Omega^{(r)}|}{|\Omega|} .$$

(D-49)

Now recalling the formal exact solution for effective permeability $\mathbf{K}^*$ which can be written as

$$(\delta \mathbf{K}^*)^{-1} = \langle \mathbf{T} \rangle^{-1} + \overline{\mathbf{G}} ,$$

(D-50)

where

$$\delta \mathbf{K}^* = \mathbf{K}^* - \mathbf{K}^{(0)} .$$

(D-51)

Multiplying Equation (D-50) with $\langle \mathbf{T}_1 \rangle$ from the left and using the standard rule for inversion of tensor inner products, it can be obtained

$$\langle \mathbf{T}_1 \rangle (\delta \mathbf{K}^*)^{-1} = \left[\langle \mathbf{T} \rangle \langle \mathbf{T}_1 \rangle^{-1} \right]^{-1} + \langle \mathbf{T}_1 \rangle \overline{\mathbf{G}} .$$

(D-52)

Combining Equations (D-43) and (D-52), it can be obtained

$$\langle \mathbf{T}_1 \rangle (\delta \mathbf{K}^*)^{-1} \approx \left[\mathbf{I} + \langle \mathbf{T}_2 \rangle \langle \mathbf{T}_1 \rangle^{-1} \right]^{-1} + \langle \mathbf{T}_1 \rangle \overline{\mathbf{G}} .$$

(D-53)

Assuming $\left\|\langle \mathbf{T}_2\rangle\langle \mathbf{T}_1\rangle\right\| << 1$, where $\|\cdot\|$ denotes a suitable tensor norm, Equation (D-52) gives

$$\langle \mathbf{T}_1\rangle(\delta \mathbf{K}_{\mathrm{T}}^{*})^{-1} = \mathbf{I} - \langle \mathbf{T}_2\rangle\langle \mathbf{T}_1\rangle^{-1} + \langle \mathbf{T}_1\rangle\overline{\mathbf{G}} \;. \tag{D-54}$$

A new expression for the tensor of effective permeability constants can be obtained from Equation (D-54) using some tensor algebra

$$\delta \mathbf{K}_{\mathrm{T}}^{*} = \langle \mathbf{T}_1\rangle(\mathbf{I} - \langle \mathbf{T}_1\rangle^{-1}\mathbf{X})^{-1}\,, \tag{D-55}$$

where

$$\mathbf{X} = \langle \mathbf{T}_2\rangle - \langle \mathbf{T}_1\rangle\overline{\mathbf{G}}\langle \mathbf{T}_1\rangle\,. \tag{D-56}$$

$\langle \mathbf{T}_1\rangle$ is given by Equation (D-44) and it remains to evaluate $\mathbf{X}$. From Equations (D-16), (D-44), (D-45), (D-46), (D-48) and (D-56), it can be obtained

$$\mathbf{X} = \sum_{\mathrm{r}}\sum_{\mathrm{s}}\mathbf{t}^{(\mathrm{r})}\left\langle \mathbf{A}^{(\mathrm{rs})}\right\rangle\mathbf{t}^{(\mathrm{s})} - \sum_{\mathrm{r}}\mathbf{t}^{(\mathrm{r})}\mathbf{v}^{(\mathrm{r})}\mathbf{G}^{(\mathrm{r})}\mathbf{t}^{(\mathrm{r})}\,, \tag{D-57}$$

where

$$\left\langle \mathbf{A}^{(\mathrm{rs})}\right\rangle = \int_{\Omega}\mathrm{d}\mathbf{x}'\mathbf{G}^{(0)}(\mathbf{x}-\mathbf{x}')\left[\left\langle \overline{\theta}^{(\mathrm{r})}(\mathbf{x})\overline{\theta}^{(\mathrm{s})}(\mathbf{x}')\right\rangle - \left\langle \overline{\theta}^{(\mathrm{r})}(\mathbf{x})\right\rangle\left\langle \overline{\theta}^{(\mathrm{s})}(\mathbf{x}')\right\rangle\right], \tag{D-58}$$

depends only on $\mathbf{K}^{(0)}$ and the stochastic geometry of the microstructure. For the evaluation of $\left\langle \mathbf{A}^{(rs)}\right\rangle$ we use the method of Jakobsen et al., (2003a) for a class of microstructures with prescribed two-point correlation functions having ellipsoidal symmetry for the distribution of the centers of arbitrarily shaped inclusions. The evaluation gives

$$\left\langle \mathbf{A}^{(\mathrm{rs})}\right\rangle = \delta_{\mathrm{rs}}\mathbf{v}^{(\mathrm{r})}\mathbf{G}^{(\mathrm{s})} - \mathbf{v}^{(\mathrm{r})}\mathbf{v}^{(\mathrm{s})}\mathbf{G}_{\mathrm{d}}^{(\mathrm{rs})}\,, \tag{D-59}$$

where

$$\mathbf{G}_{d}^{(rs)} = \int_{\Omega_{d}^{(rs)}} d\mathbf{x}' \mathbf{G}^{(0)}(\mathbf{x} - \mathbf{x}'), \qquad \mathbf{x} \in \Omega_{d}^{(rs)}, \qquad (D\text{-}60)$$

is a spatially invariant tensor since $\Omega_{d}^{(rs)}$ represents an ellipsoid having the same symmetry as $p^{(s|r)}(\mathbf{z} - \mathbf{z}')$ which, in turn, represent the probability density for finding an inclusion of type s centered at point $\mathbf{z}'$ given that there is an inclusion at point $\mathbf{z}$. From Equations (D-57) and (D-59), it can be found

$$\mathbf{X} = -\sum_{r}\sum_{s} \mathbf{t}^{(r)} \mathbf{v}^{(r)} \mathbf{G}_{d}^{(rs)} \mathbf{t}^{(s)} \mathbf{v}^{(s)}. \qquad (D\text{-}61)$$

From Equations (D-44), (D-51), (D-55) and (D-61) it follows that

$$\mathbf{K}_{T}^{*} = \mathbf{K}^{(0)} + \sum_{r} \mathbf{t}^{(r)} \mathbf{v}^{(r)} \left[\mathbf{I} + (\sum_{s} \mathbf{t}^{(s)} \mathbf{v}^{(s)})^{-1} \sum_{u}\sum_{v} \mathbf{t}^{(u)} \mathbf{v}^{(u)} \mathbf{G}_{d}^{(uv)} \mathbf{t}^{(v)} \mathbf{v}^{(v)} \right]^{-1}, \qquad (D\text{-}62)$$

which becomes completely explicit and easy to use when the inclusions are ellipsoidal in shape. Equation (D-62) can be further rewritten as

$$\mathbf{K}_{T}^{*} = \mathbf{K}^{(0)} + \sum_{r} \mathbf{t}^{(r)} \mathbf{v}^{(r)} - \sum_{r}\sum_{s} \mathbf{t}^{(r)} \mathbf{v}^{(r)} \mathbf{G}_{d}^{(rs)} \mathbf{t}^{(s)} \mathbf{v}^{(s)} + O\big[(\mathbf{v}^{(r)})^{3}\big], \qquad (D\text{-}63)$$

which is similar to the Equation (A-60) describing the effective stiffness tensor.